J Nanopart Res (2016) 18:295
DOI 10.1007/s11051-016-3587-7

DISCUSSION

Determining the composition of gold nanoparticles: a compilation of shapes, sizes, and calculations using geometric considerations

Taizo Mori · Torsten Hegmann

Received: 11 July 2016 / Accepted: 3 September 2016 / Published online: 3 October 2016

Abstract Size, shape, overall composition, and surface functionality largely determine the properties and applications of metal nanoparticles. Aside from well-defined metal clusters, their composition is often estimated assuming a quasi-spherical shape of the nanoparticle core. With decreasing diameter of the assumed circumscribed sphere, particularly in the range of only a few nanometers, the estimated nanoparticle composition increasingly deviates from the real composition, leading to significant discrepancies between anticipated and experimentally observed composition, properties, and characteristics. We here assembled a compendium of tables, models, and equations for thiol-protected gold nanoparticles that will allow experimental scientists to more accurately estimate the composition of their gold nanoparticles using TEM image analysis data. The estimates obtained from following the routines described here will then serve as a guide for further analytical characterization of as-synthesized gold nanoparticles by other bulk (thermal, structural, chemical, and compositional) and surface characterization techniques. While the tables, models, and equations are dedicated to gold nanoparticles, the composition of other metal nanoparticle cores with face-centered cubic lattices can easily be estimated simply by substituting the value for the radius of the metal atom of interest.

Keywords Gold nanoparticle · Nanocluster · Nanoparticle size · Nanoparticle shape · Nanoparticle composition · Modeling and simulation

Electronic supplementary material The online version of this article (doi:10.1007/s11051-016-3587-7) contains supplementary material, which is available to authorized users.

T. Mori · T. Hegmann (✉)
Chemical Physics Interdisciplinary Program, Liquid Crystal Institute, Kent State University, Kent, OH 44242-0001, USA
e-mail: MORI.Taizo@nims.go.jp

T. Hegmann
e-mail: thegmann@kent.edu

T. Mori
World Premier International (WPI) Research Center for Materials Nanoarchitectonics (MANA), National Institute for Materials Science (NIMS), 1-1 Namiki, Tsukuba 305-0044, Japan

List of symbols

Polyhedron

L Edge length of polyhedron
V Volume of polyhedron
S Surface area of polyhedron

Platonic and archimedean solids

R_c Circumscribed radius
R_m Midscribed radius
R_i Inscribed radius
V_{Rc} Volume of sphere with circumscribed radius (R_c)

V_{Rm} Volume of sphere with midscribed radius (R_m)
V_{Ri} Volume of sphere with inscribed radius (R_r)
S_{Rc} Surface area of sphere with circumscribed radius (R_c)
S_{Rm} Surface area of sphere with midscribed radius (R_m)
S_{Ri} Surface area of sphere with inscribed radius (R_r)

Catalan solids

a Edge length of dual solid in Catalan solids
R_v Vertex radius
R_e Edge-scribed radius
R_i Inscribed radius
V_{Rv} Volume of sphere with vertex radius (R_v)
V_{Re} Volume of sphere with edge-scribed radius (R_e)
V_{Ri} Volume of sphere with inscribed radius (R_r)
S_{Rv} Surface area of sphere with vertex radius (R_v)
S_{Re} Surface area of sphere with edge-scribed radius (R_e)
S_{Ri} Surface area of sphere with inscribed radius (R_r)

Parameter in cluster

n Generation of gold nanoparticle
D Diameter of gold nanoparticle
L Edge length of polyhedron (cluster)
L_{ico} Edge length of icosahedron
r_{Au} Radius of gold atom = 1.44 Å
R_{cs} Circumscribed radius for an icosahedron
R_c Circumscribed radius
R_m Midscribed radius
R_i Inscribed radius
D_c Circumscribed diameter = $2R_c$
D_m Midscribed diameter = $2R_m$
D_i Inscribed diameter = $2R_i$
V_{NP} Volume of gold nanoparticle
V_{Au} Volume of gold atom = 17 Å^3
V_{ico} Volume of icosahedron
N_{cs} Number of gold atoms in a circumscribed sphere for an icosahedron
N_{ico} Number of gold atoms in a regular icosahedron
M_N Magic number for gold cluster
V Volume of polyhedron (cluster)
a Edge length of dual solid in Catalan solids
R_v Vertex radius
R_e Edge-scribed radius
N_{Au} Number of gold atoms calculated assuming a quasi-spherical gold nanoparticle shape
N_{ve} Number of gold atoms calculated from volume of sphere with vertex radius (N_{ve}) = V_{Rv}/V_{Au}
N_{es} Number of gold atoms calculated from volume of sphere with edge-scribed radius (N_{es}) = V_{Re}/V_{Au}
N Number of gold atoms in cluster
N_v Number of gold atoms calculated from volume of polyhedron = V/V_{Au} (V_{Au}: volume of gold atom = 17 Å^3)
N_c Number of gold atoms calculated from volume of sphere with circumscribed radius (R_c) = V_{Rc}/V_{Au}
N_m Number of gold atoms calculated from volume of sphere with midscribed radius (R_m) = V_{Rm}/V_{Au}
N_i Number of gold atoms calculated from volume of sphere with inscribed radius (R_i) = V_{Ri}/V_{Au}
S_c Surface area of core
N_L Number of ligands on the core surface
ρ_L Ligand density

Decahedron

h Height of decahedron
w Width of decahedron
N_e Number of gold atom calculated from volume of ellipsoid
S_{Pe} Surface area of pentagonal decahedron
S_{Ino} Surface area of Ino's decahedron
S_{Ma} Surface area of Marks' decahedron

Introduction

Gold nanoparticles are everywhere! Aside from the curious and beautiful historic uses as colloidal additives to stain Roman glass in the fourth century and the discovery of the wondrous and different properties of colloidal gold by Michael Faraday in the mid nineteenth century (Tweney et al. 2004), gold nanoparticles and nanoclusters have penetrated almost every facet of science. Each year there are numerous educational and critical reviews on the use and study of gold nanoparticles for topics including in vitro diagnostics (Aillon et al. 2009; Almeida et al. 2011; Azzazy et al. 2006; Johnston et al. 2010; Khlebtsov and Dykman 2011; Mulder et al. 2009; Rosi and Mirkin 2005; Wolinsky and Grinstaff 2008), cancer diagnostics and therapy (Bhattacharyya et al. 2011; Chikkaveeraiah et al. 2012;

Dreaden et al. 2011; Gindy and Prud'homme 2009; Jain et al. 2012; Kennedy et al. 2011; Lal et al. 2008; Perfezou et al. 2012; Wang and Thanou 2010; Yong et al. 2009; Zhang et al. 2013), biological and chemical sensors (Askim et al. 2013; Howes et al. 2014; Kim et al. 2012; Perfezou et al. 2012; Pingarron et al. 2008; Sepulveda et al. 2009; Stewart et al. 2008), catalysis (Crooks et al. 2001; Hou and Cronin 2013; Panigrahi et al. 2007; Sarina et al. 2013), gold *meta*-atoms for metamaterials (Ross et al. 2016), self-assembly (Bishop et al. 2009; Boeker et al. 2007; Grzelczak et al. 2010; Lin et al. 2006; Ofir et al. 2008), intrinsic chirality (Ben-Moshe et al. 2013; Gautier and Bürgi 2009; Guerrero-Martínez et al. 2011; Wang et al. 2013; Xia et al. 2011), and this list could go on. Mind you, 20 years after the beautiful and simple Brust-Schiffrin synthesis methods (Brust et al. 1994, 1995) were published we are finding it increasingly difficult to summarize the contents of review articles, not even individual papers, on gold nanoparticles. Our group, working on understanding interactions between functionalized gold nanoparticles and soft condensed matter, even added a few to this list of reviews, summarizing studies on these magnificent nanomaterials as versatile additives in liquid crystal phases (Hegmann et al. 2007; Qi and Hegmann 2008; Shivakumar et al. 2011; Stamatoiu et al. 2012). The search for "gold nanoparticle" in Thomson Reuters Web of Science shows an ever-increasing number of papers (several thousand), and just looking at the last couple of years, a Google search leads to a mind-boggling number of over 1.8 million hits. Numerous established chemical suppliers as well as smaller startup companies now sell gold nanoparticles, but the majority of laboratories it seems still enjoy synthesizing their own, partially perhaps for educational reasons, mainly most likely for their need of specific surface functionalization toward specific application- or research-driven size or shape requirements. We are not going to summarize these synthetic efforts here, largely because, as you can easily imagine, multiple review articles heretofore did exactly that already (Alexandridis 2011; Crooks et al. 2001; Ganguli et al. 2010; Gopidas et al. 2003; Grzelczak et al. 2008; Lohse and Murphy 2013; Lu et al. 2009; Mourdikoudis and Liz-Marzan 2013; Shan and Tenhu 2007; Walther and Mueller 2013; Zhao et al. 2013; Zhou et al. 2009).

The goal of this compendium of gold nanoparticle tables, which list and compare models to more precisely calculate size and composition, is to be there for the experimentalist once the synthesis is done, and when the characterization of the just prepared precious gold nanoparticles begins. Several groups have recently shown that precise nanoclusters (magic-numbered or not) can be made exclusively, or isolated from batches with initially wider size and shape distribution, with great reproducibility (vide infra). These synthesis pathways become more and more refined, as indicated by the increasing number of articles describing new clusters. Aided by high-resolution X-ray diffraction, mass spectrometry, single-particle (a combination of low dose and aberration-corrected) transmission electron microscopy (TEM) (Azubel et al. 2014), electrophoretic mobility calculations and electromigration (Pyell 2010), thermogravimetric analysis (TGA), elemental analysis, NMR, small-angle X-ray scattering, as well as an array of surface characterization techniques (Auger, AFM, XPS, etc.) (Baer et al. 2010), these gold nanoclusters can now be fully characterized and their composition unambiguously determined. However, most laboratories and research endeavors do not require the rigor and use of well-defined gold nanoclusters. In these cases, average size and well-defined surface chemistries are more critical as is the determination of the overall, yet average composition for a gold nanoparticle sample with a given size and likely shape distribution. The functions these nanoparticles need to perform, for example as plasmonic additives, in drug delivery, in biosensing, as surface-enhanced Raman probes, among many others, do nevertheless require a precise knowledge of the nanoparticle composition. Reproducibility is a great concern for biological and medical applications as well as various other uses in device technologies, affecting performance, reliability, and last but not least intellectual property (IP). To assist in this process and create a practical go-to guide to more precisely determine the core and, in part, ligand shell composition of synthesized nanoparticles, we collected and calculated compositions and best approximations and assembled these datasets based on the overall nanocluster shape. With more and more refined and higher-resolution transmission electron microscopy (TEM) instrumentation available on the market, experimentalists should be in a position to more accurately determine their nanoparticle core composition using the nanoparticle shape revealed by TEM and using the datasets and calculations collected in the tables to come.

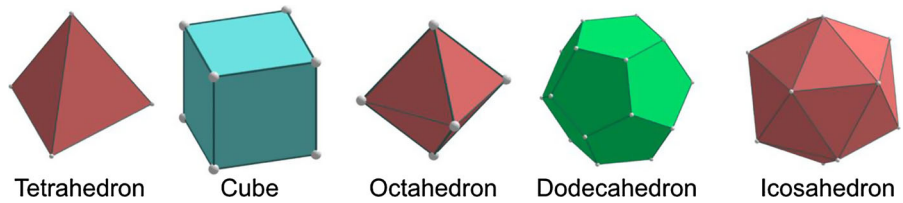

Fig. 1 Five most relevant Platonic solids: Platonic solids are polyhedra whose faces are congruent regular polygons, where the same number of faces meets at every vertex

The ligand shell is slightly more complicated. Thiolate-protected gold nanoparticles and nanoclusters dominate the literature by a large margin, and the presence of $(RS–Au(I)–SR)^-$ and $[RS(Au(I)–SR)_2]^-$ "staple" and bridge motifs (Pensa et al. 2012) (better described as Au(0)-thiyl surface bonding (Reimers et al. 2016)) largely governed by the synthesis method as well as the size and shape of the particle or cluster complicates a precise prediction or calculation of the full composition of a given thiolate-capped gold nanoparticle sample. With analytical methods such as NMR (before and after I_2 decomposition; i.e., oxidation of thiolates to disulfides), TGA, X-ray photoelectron spectroscopy (XPS) to the rescue, this hurdle can be overcome once the nanoparticle core composition is determined with some degree of precision.

First, however, we will provide an overview of the various polyhedral shapes relevant for gold nanoparticles. Most gold nanoparticles assumed to be quasi-spherical are in fact Platonic, Archimedean, or Catalan solids. Polyhedral gold nanoclusters are classified as icosahedra and face-centered cubic (fcc) polyhedra. The stable Ino's and Marks' decahedra are non-spherical shapes and are best described as ellipsoids. The icosahedral or Ino's as well as Marks' decahedral-based gold nanoclusters (with icosahedral structure considering the triangular faces and fcc structure when considering the rectangular faces) represent more molecular-like structures. The fcc-based gold nanoparticles have more bulk (plasmonic) structures.

There are five platonic solids constructed by regular polygonal faces (Fig. 1), with tetrahedron, cube, and octahedron combined known as fcc unit cell substructures. Magic-numbered gold nanoclusters have regular icosahedral shapes.

Two or three regular polygonal faces are needed to construct Archimedean solids, and truncating Platonic solids can compose them. As a result, Archimedean solids that are truncated from either tetrahedron, cube, or octahedron have fcc structures; other Archimedean solids have icosahedral structures as graphically shown in Fig. 2.

The process of obtaining these Archimedean solids by truncation is graphically shown in Fig. 3. The remaining Catalan solids are defined as dual solids of Archimedean solids. As their faces are not regular polygonal, it is expected that the cores of metal clusters could not be Catalan solid structures; however, ligand shells of Archimedean metal clusters could have Catalan solid structures (Fig. 4).

Tables, models, and calculations

Spherical versus icosahedral model

The number of gold atoms N_{Au} is commonly calculated assuming a quasi-spherical gold nanoparticle shape using Eq. 1 (Leff et al. 1995):

$$N_{Au} = \frac{4\pi r^3}{3V_{Au}} = \frac{\pi D^3}{102} \quad (1)$$

where V_{Au} is the volume of the Au atom ($V_{Au} = 17$ Å^3), r and D are the radius and the diameter of the gold nanoparticle, respectively, and r_{Au} is the radius of the gold atom ($r_{Au} = 1.44$ Å) with $r = (2n + 1)r_{Au}$, where n is the number of full gold atoms along the radius of the nanoparticle as shown in Fig. 5.

As the size of the gold nanoparticles change (decrease or increase), and polyhedral shapes of specific clusters are now increasingly synthetically accessible, the use of this simple model becomes, as we will see, more and more problematic. Figure 6 shows that with the progression from a larger to a smaller nanoparticle (or cluster) the assumption of a quasi-spherical nanoparticle leads to a larger and larger discrepancy in composition.

For the calculation we first introduce the radius of the circumscribed sphere for an icosahedron R_{cs}. For a

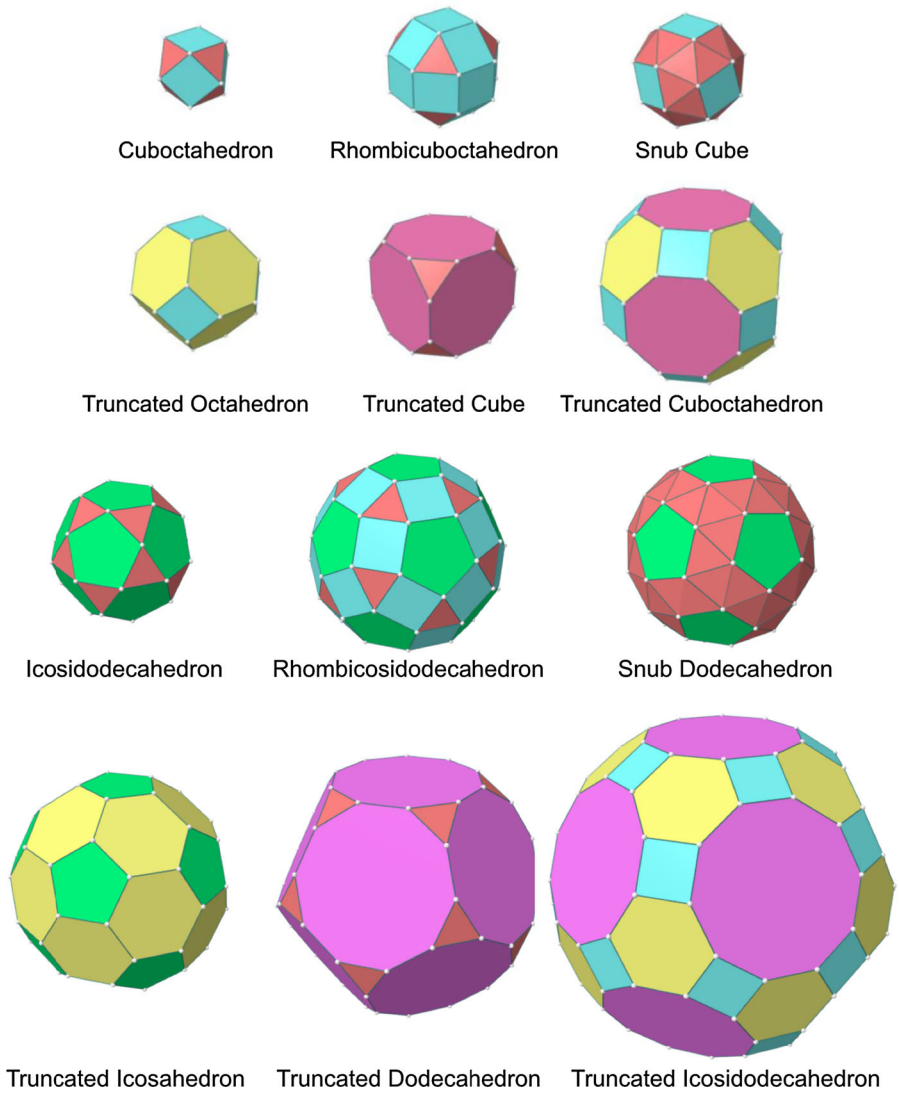

Fig. 2 Depiction of several highly symmetric Archimedean solids with semi-regular color-coded regular polygonal faces

Au_{55} cluster, this leads to $R_{cs} = 7.2$ Å and a diameter of $D = 1.44$ nm as shown in Fig. 7. For magic-numbered gold clusters, whose overall shape is best described as regular icosahedral, the following equations give the number of gold atoms in a regular icosahedron N_{ico} (Eq. 2), the radius of the circumscribed sphere for an icosahedron R_{cs} (Eq. 3), and the magic number M_N (Eq. 4):

$$N_{ico} = \frac{V_{ico}}{V_{Au}} \tag{2}$$

$$R_{cs} = \frac{\sqrt{10 + 2\sqrt{5}}}{4} L_{ico} \tag{3}$$

$$M_N = \frac{1}{3}(2n + 1)\left(5n^2 + 5n + 3\right) \tag{4}$$

where V_{ico} is the volume of the icosahedron, V_{Au} the volume of the gold atom, L_{ico} the edge length of the icosahedron, and where $R_{cs} = (2n + 1)r_{Au}$ as mentioned earlier. For the magic-sized clusters with $n = 1$–5, this results in a composition of these clusters as shown in Fig. 8.

Table 1 lists the values and Fig. 9 graphically shows the obvious discrepancies between a quasi-spherical model and the regular icosahedral shape and the comparison of the number of gold atoms obtained for both shapes, where the values of N_{cs} (the number of

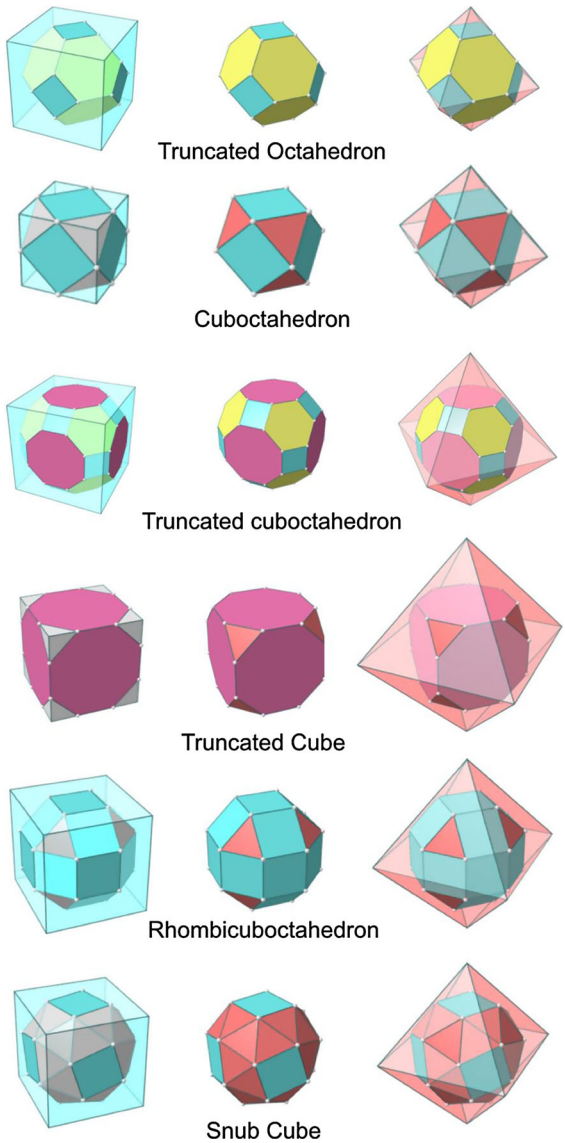

Fig. 3 Truncation of Platonic solids with Platonic solids leads to Archimedean solids

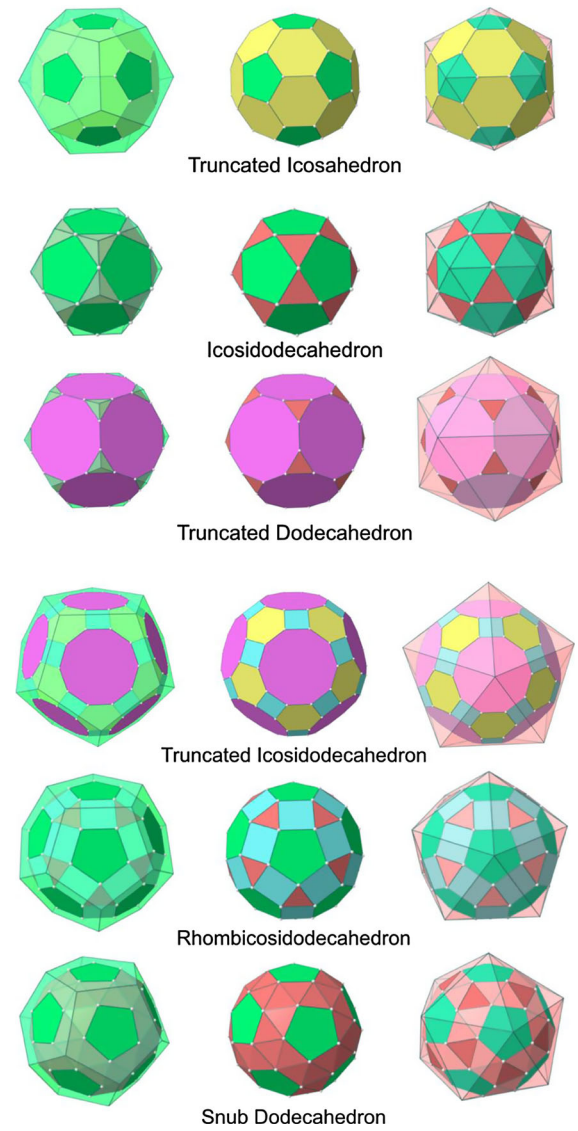

Fig. 3 continued

gold atoms obtained from the radius of the circumscribed sphere) and N_{ico} (the number of gold atoms in the regular icosahedron) divided by the magic number M_N should be close to 1 for a match between experiment and calculation. As one can see, this number quickly and rather drastically deviates when a quasi-spherical model is used. For example, for nanoparticles in the size range of 2–3 nm, which are frequently described in the literature, the quasi-spherical model overestimates the number of gold atoms by a factor of over 1.7.

The magnitude of deviation between the number of gold atoms in a nanoparticle or nanocluster varying with the use of either the quasi-spherical or more accurate polyhedral model largely depends on the shape of individual particles. High-resolution transmission electron microscopy (HR-TEM) is nowadays more than capable of revealing precise nanoparticle shapes and sizes, particularly when coupled with TEM tomography. Exact calculation of the nanoparticle composition should therefore be rather straightforward using the equations for the various polyhedral shapes provided in Section S1 of the Electronic

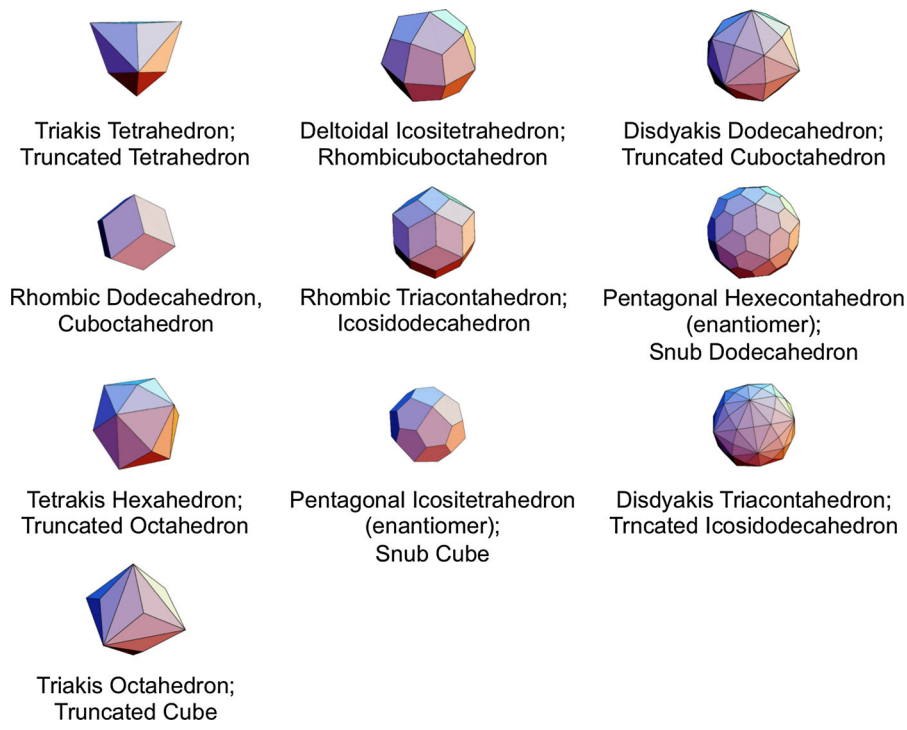

Fig. 4 Depiction of Catalan solids defined as dual solids of Archimedean solids (the name of both Catalan solid and the dual solid is provided). Catalan solids are characterized by faces with non-equal edge lengths. Models taken from: Wolfram MathWorld; http://mathworld.wolfram.com

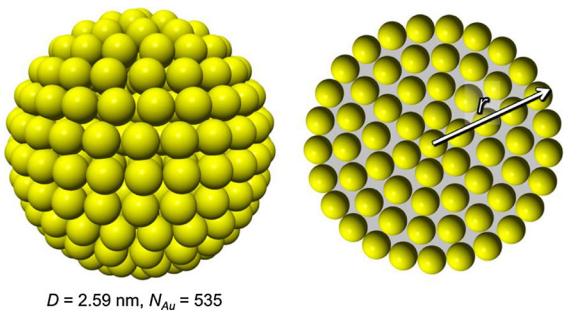

Fig. 5 A quasi-spherical representation of a Au_{535} cluster used to demonstrate the estimation of the gold nanocluster size and composition via the frequently used quasi-spherical model

Supplementary Material (ESM). Table S2A expands on the comparison between the quasi-spherical model and models of many other polyhedral shapes that are, or could be, formed by gold (or other coinage metal) nanoparticles or clusters for a specific radius of the circumscribed sphere of $R_c = 10.08$ Å (related to a Au_{147} cluster with regular icosahedral shape). We again provide a measure of the goodness of fit between the quasi-spherical and the given polyhedral model by the ratio between the number of gold atoms obtained from each model N_c/N_v, where N_c is again the number of gold atoms contained within the circumscribed sphere and N_v is the number of gold atoms calculated from the volume of the polyhedron. For Catalan solids N_{ve} is the number of gold atoms calculated from the volume of the sphere with vertex radius ($N_{ve} = V_{Rv}/V_{Au}$) calculated from the volume of the sphere with vertex radius in Catalan solids (V_{Rv}). A related table showing the discrepancies between the quasi-spherical model and specific polyhedral shapes assuming a radius of the circumscribed sphere of $R_c = 7.2$ Å (related to a Au_{55} cluster with regular icosahedral shape) is given in the ESM (Section S2, Table S2B).

Decahedral model

Jiang et al. (2003) Now that we have general sense of the influence of the nanoparticle or nanocluster shape, we will look at specific and commonly found polyhedral nanocluster shapes and calculate the composition of the clusters depending on the specific sub-type and size. Specifically, we will look at decahedra, Archimedean cubes, and Archimedean icosahedra. Table 2 provides a complete list of pentagonal decahedra, Ino's decahedra, and Marks' decahedra by generation (layers of gold atoms around the center atoms) giving

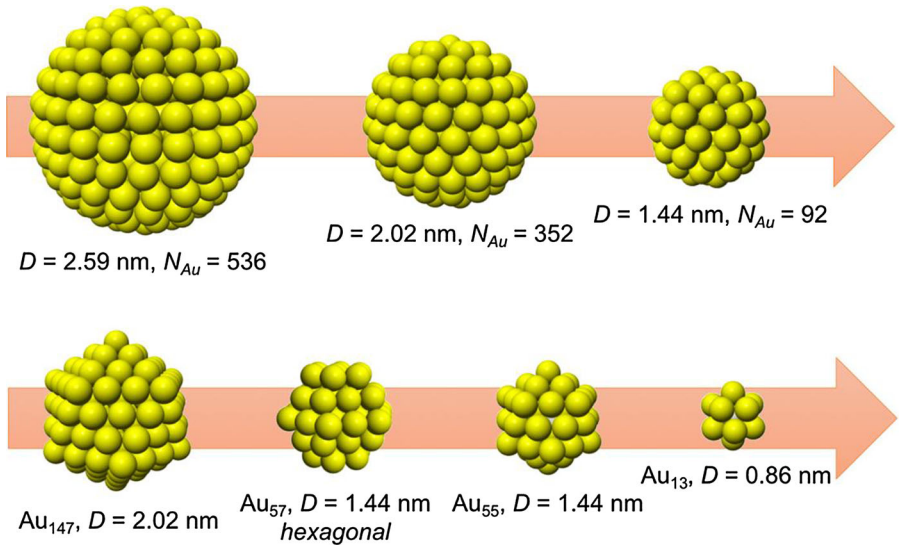

Fig. 6 Shape determines composition: The *graphic* shows how as the size of the gold nanoparticle decreases and polyhedral shapes of well-defined clusters dominate, the spherical model to calculate the gold nanoparticle composition is less and less accurate

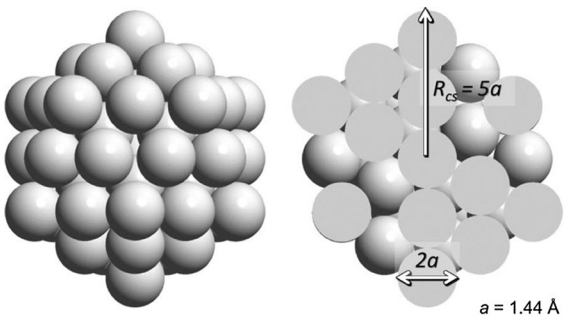

Fig. 7 Full and cross-sectional view of a Au_{55} cluster highlighting the radius of the circumscribed sphere in the quasi-spherical model

the number of gold atoms at the surface, the total number of gold atoms of the cluster, the parent cluster that is covered with another layer of gold atoms as well as their calculated heights and widths. Pentagonal decahedra are composed of ten faces of icosahedra. Ino's and Marks' decahedra are created by truncating pentagonal decahedra. Thus, these decahedra have icosahedral structures on triangular faces and fcc structures on rectangular faces.

A more condensed view of these values is given in Table 3, also providing additional generation 4 (G4) clusters. The number of gold atoms calculated assuming an ellipsoidal shape (N_e) of the overall cluster is given in Eq. 5 (h, r_{Au}, and w are defined in Table 2).

$$N_e = \frac{4\pi}{3V_{Au}} \frac{h - r_{Au}}{2} \left(\frac{w - r_{Au}}{2}\right)^2 \quad (5)$$

Divided by the precise number of gold atoms in the cluster, the ratio of N_e/N shows how close an elliptical particle shape assumption would be as the size of the cluster increases, especially in the absence of high-resolution TEM images or X-ray diffraction data that would allow the experimentalist to deduce the exact particle shape and composition.

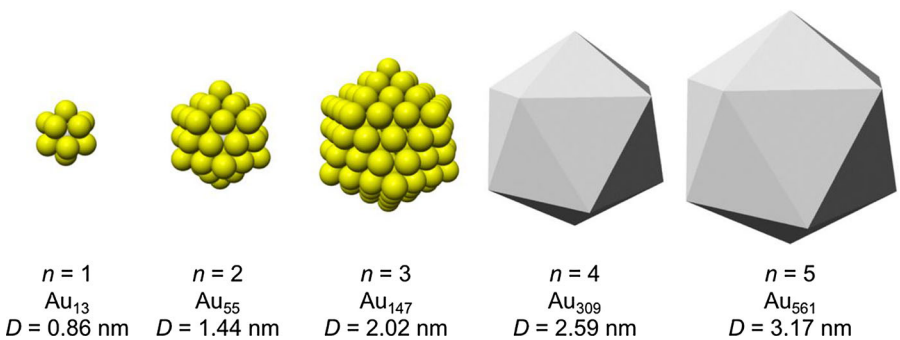

Fig. 8 Magic-numbered gold clusters and their composition and diameter calculated assuming a regular icosahedral shape

Table 1 Comparison of the number of gold atoms using a quasi-spherical and a more precise icosahedral model

n	M_N	R_{cs}/Å	D/nm	L_{ico}/Å	V_{ico}/Å^3	N_{cs}	N_{ico}	N_{cs}/M_N	N_{ico}/M_N
1	13	4.32	0.86	4.54	204.34	19.9	12.0	1.528	0.925
2	55	7.2	1.44	7.57	946.04	92.0	55.6	1.672	1.012
3	147	10.08	2.02	10.60	2595.95	252.4	152.7	1.717	1.039
4	309	12.96	2.59	13.63	5517.34	536.4	324.5	1.736	1.050
5	561	15.84	3.17	16.66	10,073.50	979.3	592.6	1.746	1.056

V_{ico} is the volume of the icosahedron, and N_{cs} and N_{ico} are the number of gold atoms in the circumscribed sphere and the regular icosahedron, respectively

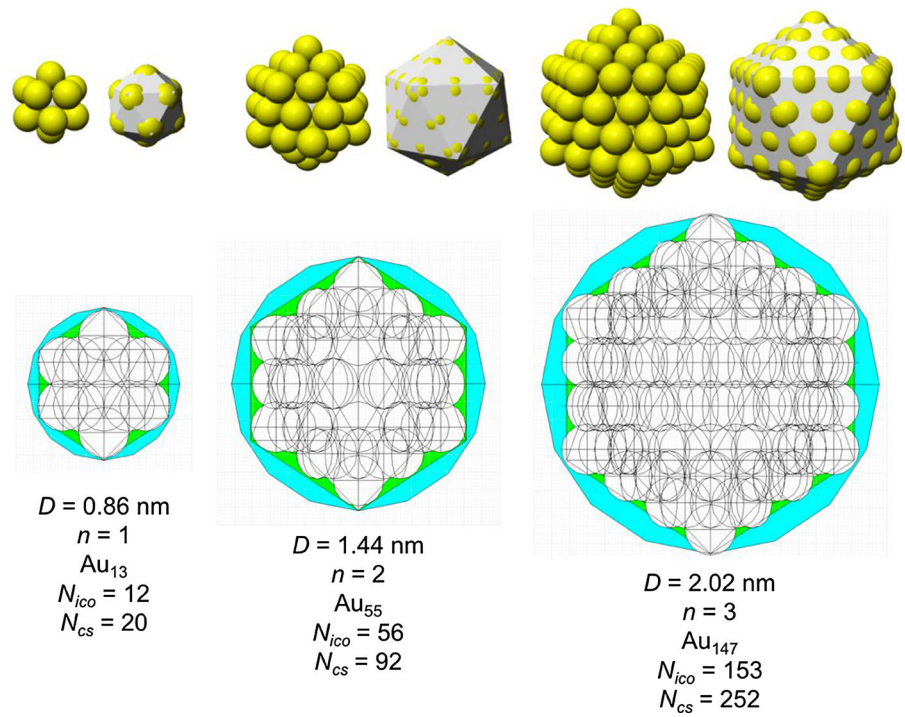

Fig. 9 Magic-numbered gold clusters with $n = 1$–3 (Au_{13}, Au_{55}, and Au_{147}) above and discrepancy in the number of gold atoms between quasi-sphere and regular icosahedron

Archimedean icosahedra model

Table 4 lists the same information for Archimedean icosahedra starting with the smallest, first-generation (G1) Au_{13} cluster. Among them, we also find several of the magic-sized gold nanoclusters with icosahedral shape such as Au_{13}, Au_{55}, Au_{147}, among others, as shown in Fig. 9.

The ratio of the number of gold atoms between calculated and ideal cluster in these Archimedean icosahedra (Table S3, Section S3) shows how the quasi-spherical model (using the diameter of the circumscribed (N_c), midscribed (N_m) or inscribed diameter (N_i) sphere), or using the number of gold atoms deduced from a polyhedral model (N_v) deviates from the correct number of gold atoms for these clusters.

Archimedean cube model

Table 5 finally shows a list of Archimedean cubes from generation 1 to 6 (G1–G6). Again, the ratio of the number of gold atoms between calculated and ideal cluster in these Archimedean cubes (Table S4, Section S4) shows how quasi-spherical models (using the diameter of the circumscribed (N_c), midscribed (N_m)

Table 2 List of generations (G1 to G4) of pentagonal decahedra, Ino's decahedra, and Marks' decahedra (number of atoms in cluster, on the surface, parent cluster, height, and width)

Marks' Decahedron

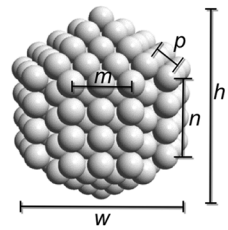

(*m*, *n*, *p*) = (3, 4, 2)

$$N = \frac{1}{6}\left\{\begin{matrix}(30p^3 135p^2 + 207p - 102)\\ +[5m^3 + (30p - 45)m^2 + (60(p^2 - 39) + 136)m]\\ +n[15m^2 + (60p - 75)m + 3(10p^2 - 30p) + 66]\end{matrix}\right\} - 1$$

Pentagonal decahedron $(n_k = 1, p_k = 1)$
$(m_{k-1}, n_{k-1}, p_{k-1}) = (m_k - 2, 1, 1)$

$Surface\ area$: $S_{Pe} = 10\left[(2r_{Au}\times m)^2 \sin\frac{\pi}{3}\right]$

Pentagonal Marks' decahedron $(n_k = 1, p_k = 2)$
$(m_{k-1}, n_{k-1}, p_{k-1}) = (m_k, 1, 1)$

Ino's decahedron $(n_k > 1, p_k = 1)$
$(m_{k-1}, n_{k-1}, p_{k-1}) = (m_k - 1, n_{k-1}n_k - 1, 1)$

$Surface\ area$: $S_{Ino} = 10\left[(2r_{Au}\times m)^2 \sin\frac{\pi}{3}\right] + 5[(2r_{Au})^2\times m\times n]$

Mark's decahedron $(n_k > 1, p_k = 2)$
$(m_{k-1}, n_{k-1}, p_{k-1}) = (m_k - 1, n_{k-1}n_k - 1, 2)$

Surface area:

$$S_{Ma} = 10\left[(2r_{Au}\times m)^2 \sin\frac{\pi}{3}\right] + 5[(2r_{Au})^2\times m\times n] + 10[(2r_{Au})^2\times n\times(p+1)]$$

$height$: $h = 2r_{Au}(m + n + 2p - 3)$

$width$: $w = \left[\frac{4(m+p-2)}{\sin\frac{\pi}{5}\sqrt{10+2\sqrt{5}}} + p\right] r_{Au}$

G1

Pentagonal Decahedron 7 (*m*, *n*, *p*) = (2, 1, 1)
Cluster 7 *h* = 0.58 nm, *w* = 0.80 nm
Surface 6
Atom 1

Ino's Decahedron 13 (*m*, *n*, *p*) = (2, 2, 1)
Cluster 13 *h* = 0.86 nm, *w* = 0.80 nm
Surface 12
Atom 1

Marks' Decahedron 18 (*m*, *n*, *p*) = (1, 1, 2)
Cluster 18 *h* = 0.86 nm, *w* = 1.09 nm
Surface 17
Atom 1

Marks' Decahedron 29 (*m*, *n*, *p*) = (1, 1, 2)
Cluster 29 *h* = 1.15 nm, *w* = 1.09 nm
Surface 27
Atom 2

G2

Pentagonal Decahedron 23 (*m*, *n*, *p*) = (3, 1, 1)
Cluster 23 *h* = 0.86 nm, *w* = 1.32 nm
Surface 22
Atom 1

Ino's Decahedron 39 (*m*, *n*, *p*) = (3, 2, 1)
Cluster 39 *h* = 1.15 nm, *w* = 1.32 nm
Surface 32
Pentagonal Decahedron 7

Marks' Decahedron 49 (*m*, *n*, *p*) = (2, 1, 2)
Cluster 49 *h* = 1.15 nm, *w* = 1.61 nm
Surface 42
Pentagonal Decahedron 7

Ino's Decahedron 55 (*m*, *n*, *p*) = (3, 3, 1)
Cluster 55 *h* = 1.44 nm, *w* = 1.32 nm
Surface 42
Ino's Decahedron 13

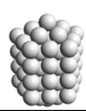

Ino's Decahedron 71 (*m*, *n*, *p*) = (3, 4, 1)
Cluster 71 *h* = 1.73 nm, *w* = 1.32 nm
Surface 52
Ino's Decahedron 19

Table 2 continued

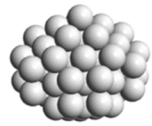	**Marks' Decahedron 75** Cluster 75 Surface 57 Marks' Decahedron 18	(*m*, *n*, *p*) = (2, 2, 2) *h* = 1.44 nm, *w* = 1.61 nm
	**Marks' Decahedron 101** Cluster 101 Surface 72 Marks' Decahedron 29	(*m*, *n*, *p*) = (2, 3, 2) *h* = 1.73 nm, *w* = 1.61 nm
G3		
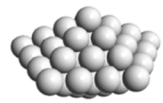	**Pentagonal Decahedron 54** Cluster 54 Surface 47 Pentagonal Decahedron 7	(*m*, *n*, *p*) = (4, 1, 1) *h* = 1.15 nm, *w* = 1.83 nm
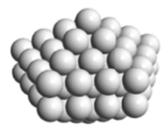	**Ino's Decahedron 85** Cluster 85 Surface 63 Pentagonal Decahedron 23	(*m*, *n*, *p*) = (4, 2, 1) *h* = 1.44 nm, *w* = 1.83 nm
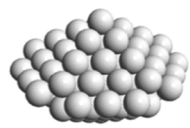	**Marks' Decahedron 100** Cluster 100 Surface 77 Pentagonal Decahedron 23	(*m*, *n*, *p*) = (3, 1, 2) *h* = 1.44 nm, *w* = 2.12 nm
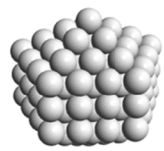	**Ino's Decahedron 116** Cluster 116 Surface 107 Ino's Decahedron 39	(*m*, *n*, *p*) = (4, 3, 1) *h* = 1.73 nm, *w* = 1.83 nm
	**Marks' Decahedron 146** Cluster 146 Surface 97 Marks' Decahedron 49	(*m*, *n*, *p*) = (3, 2, 2) *h* = 1.73 nm, *w* = 2.12 nm
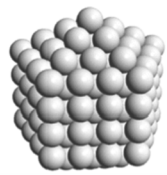	**Ino's Decahedron 147** Cluster 147 Surface 92 Ino's Decahedron 55	(*m*, *n*, *p*) = (4, 4, 1) *h* = 2.02 nm, *w* = 1.83 nm

Table 2 continued

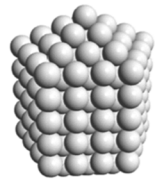	**Ino's Decahedron 178** Cluster 178 Surface 107 Ino's Decahedron 71	(*m*, *n*, *p*) = (4, 5, 1) *h* = 2.30 nm, *w* = 1.83 nm
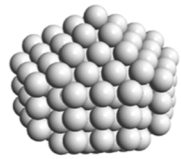	**Marks' Decahedron 192** Cluster 192 Surface 117 Marks' Decahedron 75	(*m*, *n*, *p*) = (3, 3, 2) *h* = 2.02 nm, *w* = 2.12 nm
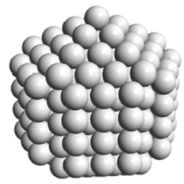	**Marks' Decahedron 238** Cluster 238 Surface 137 Marks' Decahedron 101	(*m*, *n*, *p*) = (3, 4, 2) *h* = 2.30 nm, *w* = 2.12 nm
G4		
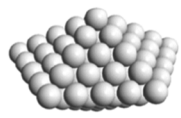	**Pentagonal Decahedron 105** Cluster 105 Surface 82 Pentagonal Decahedron 23	(*m*, *n*, *p*) = (5, 1, 1) *h* = 1.44 nm, *w* = 2.35 nm
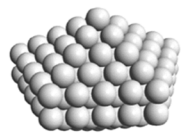	**Ino's Decahedron 156** Cluster 156 Surface 102 Pentagonal Decahedron 54	(*m*, *n*, *p*) = (5, 2, 1) *h* = 1.73 nm, *w* = 2.35 nm
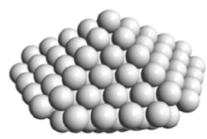	**Marks' Decahedron 176** Cluster 176 Surface 122 Pentagonal Decahedron 54	(*m*, *n*, *p*) = (4, 1, 2) *h* = 1.73 nm, *w* = 2.64 nm

The parameters and equations used are shown at the top of the table

or inscribed diameter (N_i) sphere), or using the number of gold atoms deduced from a polyhedral model (N_v) deviate from the correct number of atoms.

Other models: defects, shell structures, and "staples"

Thus far, we have provided calculations and models for regular polyhedral shapes of gold nanoparticles. However, these models do not include specifics of shell structures (the outer layer of gold atoms involved in thiolate ligand binding), but we can estimate the number of gold-thiolate "staple" and bridge motifs by calculating the ligand density at the gold nanoparticle surface.

Particularly, the cores of chiral gold nanoparticles consist of non-regular polyhedral structures and usually exhibit defects in their crystal structures (Chen et al. 2015; Dolamic et al. 2012; Kimura et al. 2009; Levi-Kalisman et al. 2011; Lopez-Acevedo et al.

Table 3 List of clusters with decahedral shape, including regular, Ino's, and Marks' decahedra

Decahedron	G	*m*	*n*	*p*	Cluster	Surface	Inner	*h*/nm	*w*/nm	N_e	N_e/N
Pentagonal decahedron 7	1	2	1	1	7	6	1	0.58	0.80	3.5	0.50
Ino's decahedron 13	1	2	2	1	13	12	1	0.86	0.80	5.9	0.45
Marks' decahedron 18	1	1	1	2	18	17	1	0.86	1.09	14.3	0.79
Marks' decahedron 29	1	1	2	2	29	27	2	1.15	1.09	20.0	0.69
Pentagonal decahedron 23	2	3	1	1	23	22	1	0.86	1.32	23.5	1.02
Ino's decahedron 39	2	3	2	1	39	32	7	1.15	1.32	33.0	0.85
Marks' decahedron 49	2	2	1	2	49	42	7	1.15	1.61	54.0	1.10
Ino's decahedron 55	2	3	3	1	55	42	13	1.44	1.32	42.4	0.77
Ino's decahedron 71	2	3	4	1	71	52	19	1.73	1.32	51.8	0.73
Marks' decahedron 75	2	2	2	2	75	57	18	1.44	1.61	69.4	0.93
Marks' decahedron 101	2	2	3	2	101	72	29	1.73	1.61	84.8	0.84
Pentagonal decahedron 54	3	4	1	1	54	47	7	1.15	1.83	74.2	1.37
Ino's decahedron 85	3	4	2	1	85	62	23	1.44	1.83	95.4	1.12
Marks' decahedron 100	3	3	1	2	100	77	23	1.44	2.12	134.2	1.34
Ino's decahedron 116	3	4	3	1	116	77	39	1.73	1.83	116.5	1.00
Marks' decahedron 146	3	3	2	2	146	97	49	1.73	2.12	164.0	1.12
Ino's decahedron 147	3	4	4	1	147	92	55	2.02	1.83	137.7	0.94
Ino's decahedron 178	3	4	5	1	178	107	71	2.30	1.83	158.9	0.89
Marks' decahedron 192	3	3	3	2	192	117	75	2.02	2.12	193.8	1.01
Marks' decahedron 238	3	3	4	2	238	137	101	2.30	2.12	223.7	0.94
Pentagonal decahedron 105	4	5	1	1	105	82	23	1.44	2.35	169.5	1.61
Ino's decahedron 156	4	5	2	1	156	102	54	1.73	2.35	207.2	1.33
Marks' decahedron 176	4	4	1	2	176	91	85	1.73	2.64	269.1	1.53
Ino's decahedron 207	4	5	3	1	207	122	85	2.02	2.35	244.9	1.18
Ino's decahedron 258	4	5	4	1	258	142	116	2.30	2.35	282.5	1.10
Ino's decahedron 309	4	5	5	1	309	162	147	2.59	2.35	320.2	1.04
Marks' decahedron 247	4	4	2	2	247	147	100	2.02	2.64	318.1	1.29
Marks' decahedron 318	4	4	3	2	318	172	146	2.30	2.64	367.0	1.15
Marks' decahedron 389	4	4	4	2	389	197	192	2.59	2.64	415.9	1.07

G generation, *m*, *n*, and *p* are defined in Table 2, and the inner cluster is the parent cluster

2010; Pei et al. 2009; Pelayo et al. 2015; Qian and Jin 2009; Takagi et al. 2015; Tlahuice-Flores et al. 2013a, b; Weissker et al. 2014; Zeng et al. 2015). Such non-regular polyhedral as well as defect structures of nanoparticle cores are generally the origin for the observed nanoparticle chirality. The core structures of several prominent chiral gold nanoparticles are summarized in Table 6.

Particularly, the cores of the smaller chiral gold nanoparticles are composed of connected regular polyhedra such as continuous tetrahedra and/or icosahedra. The core of Au_{68}(3-MBA)$_{50}$ features 50 gold atoms formed from an Archimedean icosahedral structure (icosidodecahedron) with defects (Pelayo et al. 2015). Similarly, the cores of both Au_{102}(*p*-MBA)$_{32}$ and Au_{133}(S-Ph-*p*–*t*-Bu)$_{52}$ were formed from rhombicosidodecahedron also with defects (Chen et al. 2015; Levi-Kalisman et al. 2011; Pelayo et al. 2015; Zeng et al. 2015). The core structure of Au_{68}(3-MBA)$_{50}$ appears to be most closely related either to an Ino's decahedron with defects or to a non-regular polyhedral Au_{53} as shown in Fig. 10 (Pelayo et al. 2015). Several other chiral gold nanoparticles have regular polyhedra cores (entries highlighted by # in Table 6). For example, the core of Au_{144}(S-R_3)$_{60}$ formed from Au_{114} (Qian and Jin 2009; Tlahuice-Flores et al. 2013a) finds its best match in the Archimedean icosahedra model as rhombicosidodecahedron Au_{115} in Table 4.

To estimate the number of gold atoms on the surface we have to calculate the ligand density (ρ_L). Table 7 shows the surface area of the nanoparticle core (S_c) as well as the ligand density for gold nanoparticles. The ligand density of $[Au_{25}(S–CH_2\text{-}CH_2Ph)_{18}]^-$ and $Au_{144}(S–CH_3)_{60}$ with Archimedean icosahedra cores, calculated using simple Eq. 6 (N_L is the number of thiolate ligands), is close to 15 Å^2, which is equal to the maximum packing density of thiolates on gold nanoparticle (Kimura et al. 2009).

$$\rho_L = \frac{S_c}{N_L} \tag{6}$$

The $Au_{144}(S\text{-}CH_3)_{60}$ cluster reported by Jin et al. (Qian and Jin 2009) has 30–S–Au–S–"staple" motifs with 30 gold and 60 sulfur atoms within the shell structure (Weissker et al. 2014). Using the same approach, we calculated that the ligand density of the $Au_{24}(S\text{-adamantane})_{16}$ cluster(Pelayo et al. 2015) with an Archimedean cube core was 19 Å^2, similar to the surface area of thiols calculated for planar gold surfaces (i.e., self-assembled monolayers on gold, SAMs (Love et al. 2005)) at 21 Å^2. This suggests that the surface of cores with Archimedean cube structure would act more like a bulk gold surface than cores with Archimedean icosahedra shape that are more faceted, which makes sense.

The cores of $Au_{54}(S–C_{18}H_{37})_{30}$ and $Au_{55}(S–C_{18}H_{37})_{31}$ were formed from Ino's decahedron 39 (Negishi et al. 2012; Tsunoyama et al. 2010). The ligand density of Ino's decahedron 39 ($\rho_L = 18.2$ Å^2) is situated between the thiol ligand density of Archimedean icosahedra gold nanoparticles ($\rho_L = 15$ Å^2) and flat gold surfaces ($\rho_L = 21$ Å^2). The reason for this is that the decahedra surfaces are formed from a combination of icosahedral core (particle like) on triangular faces and cubic core (bulk like) on rectangular faces.

The core structure of the $Au_{187}(S–C_{12}H_{25})_{68}^{15}$ has been elucidated by density functional theory (DFT) calculations as a Marks' decahedron Au_{153} (Tlahuice-Flores 2015). It is conceivable that $Au_{187}(S\text{-}C_{12}H_{25})_{68}$ clusters have either a truncated cuboctahedron 135 or a cuboctahedron 147 core structure considering the models listed in Table 5. The ligand densities of the $Au_{187}(S–C_{12}H_{25})_{68}$ cluster were calculated for each possible core (Table 7).

The ligand densities of a Marks' decahedral Au_{153}, a truncated cuboctahedron 135, and a cuboctahedron 147 amount to 16.6, 14.1, and 15.9 Å^2, respectively. The values of the ligand densities obtained for the truncated cuboctahedron 135 and the cuboctahedron 147 suggest that thiolate ligands are more tightly packed on these clusters than thiolates on gold SAMs (21 Å^2). Thus, the core of the $Au_{187}(S–C_{12}H_{25})_{68}$ should be neither a truncated cuboctahedron 135 nor a cuboctahedron 147, because the ligand density of a particle core with Archimedean cube structure should be closer to the surface area of thiolates on a flat gold SAM. Thus, the core structure of the $Au_{187}(S–C_{12}H_{25})_{68}$ should be based on a Marks' decahedral Au_{153} as determined by the authors experimentally.

Qian et al. (2012) reported on the core of a $Au_{333}(S\text{-}CH_2CH_2Ph)_{79}$ cluster formed from fcc Au_{293}. We can suggest other possible core structures from the models summarized in the tables. The ligand densities of cores with Archimedean cube structure such as sub-truncated cuboctahedron 297, cuboctahedron 309, sub-truncated octahedron 314 were calculated to be 22 Å^2, closely matching with the surface area of thiolates on gold SAMs. The ligand densities of cores with decahedral structure such as Ino's decahedron 309 and Marks' decahedron 318 are 15 Å^2, which is close to that of the $Au_{187}(S–C_{12}H_{25})_{68}$ cluster formed from a Marks' decahedral Au_{153}. The authors considered sub-truncated cuboctahedron 297 or cuboctahedron 309 as core structure of the $Au_{333}(S–CH_2CH_2Ph)_{79}$ cluster, but a sub-truncated octahedron 314, an Ino's decahedron 309, and a Marks' decahedron 318 should be reconsidered as the most likely core structures based on ligand density values. These examples show how the tables, calculations, and consideration of ligand densities can be used to determine the core structure of gold nanoparticles. The following part will provide a quick how-to guide.

Using the tables

Now that we have the tabulated data for the various models, it is time to put them to the test. First, we provide a point-by-point procedure how to use these

Table 4 List of generations (G1 to G6) of Archimedean icosahedra (number of atoms in cluster, on the surface, parent (inner) cluster, height, and width

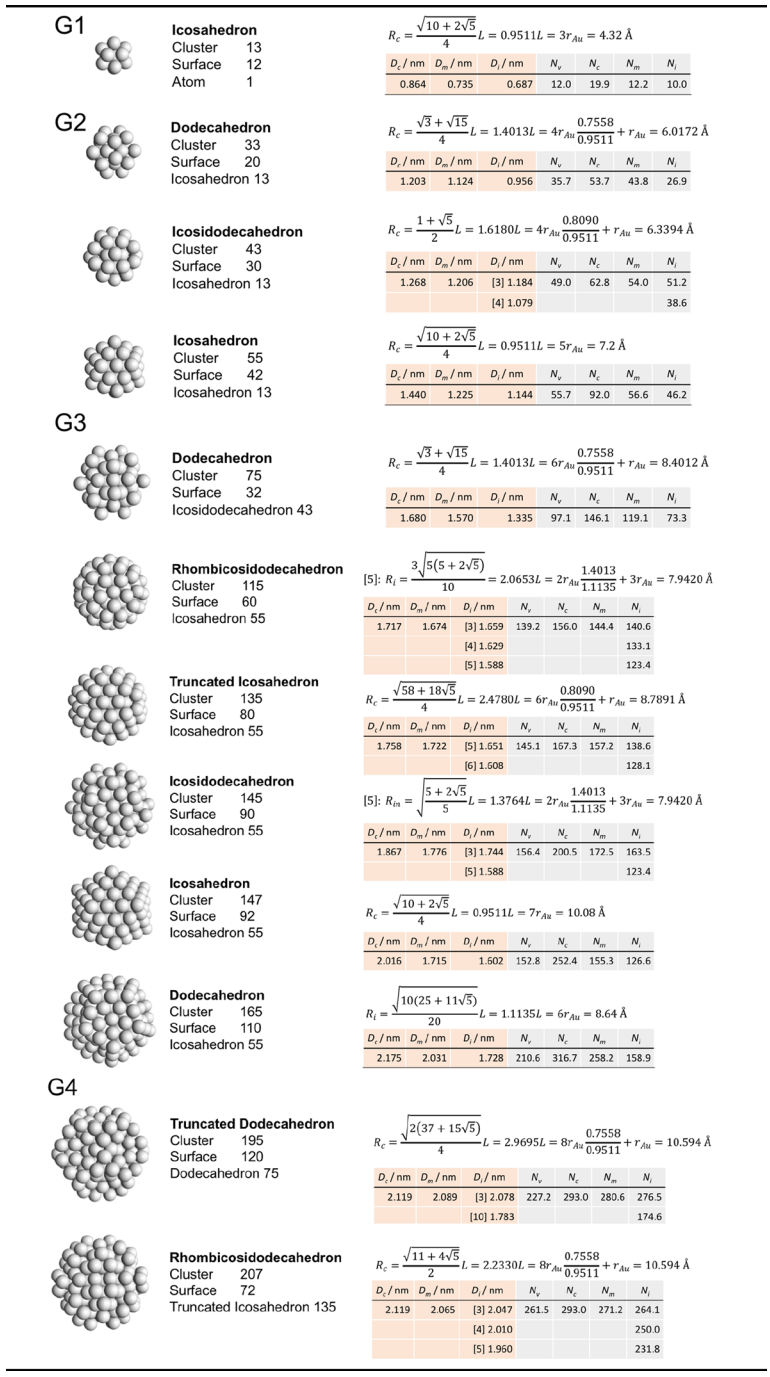

G1

Icosahedron
Cluster 13
Surface 12
Atom 1

$R_c = \frac{\sqrt{10+2\sqrt{5}}}{4} L = 0.9511L = 3r_{Au} = 4.32$ Å

D_c / nm	D_m / nm	D_i / nm	N_v	N_c	N_m	N_i
0.864	0.735	0.687	12.0	19.9	12.2	10.0

G2

Dodecahedron
Cluster 33
Surface 20
Icosahedron 13

$R_c = \frac{\sqrt{3}+\sqrt{15}}{4} L = 1.4013L = 4r_{Au}\frac{0.7558}{0.9511} + r_{Au} = 6.0172$ Å

D_c / nm	D_m / nm	D_i / nm	N_v	N_c	N_m	N_i
1.203	1.124	0.956	35.7	53.7	43.8	26.9

Icosidodecahedron
Cluster 43
Surface 30
Icosahedron 13

$R_c = \frac{1+\sqrt{5}}{2} L = 1.6180L = 4r_{Au}\frac{0.8090}{0.9511} + r_{Au} = 6.3394$ Å

D_c / nm	D_m / nm	D_i / nm	N_v	N_c	N_m	N_i
1.268	1.206	[3] 1.184	49.0	62.8	54.0	51.2
		[4] 1.079				38.6

Icosahedron
Cluster 55
Surface 42
Icosahedron 13

$R_c = \frac{\sqrt{10+2\sqrt{5}}}{4} L = 0.9511L = 5r_{Au} = 7.2$ Å

D_c / nm	D_m / nm	D_i / nm	N_v	N_c	N_m	N_i
1.440	1.225	1.144	55.7	92.0	56.6	46.2

G3

Dodecahedron
Cluster 75
Surface 32
Icosidodecahedron 43

$R_c = \frac{\sqrt{3}+\sqrt{15}}{4} L = 1.4013L = 6r_{Au}\frac{0.7558}{0.9511} + r_{Au} = 8.4012$ Å

D_c / nm	D_m / nm	D_i / nm	N_v	N_c	N_m	N_i
1.680	1.570	1.335	97.1	146.1	119.1	73.3

Rhombicosidodecahedron
Cluster 115
Surface 60
Icosahedron 55

[5]: $R_i = \frac{3\sqrt{5(5+2\sqrt{5})}}{10} = 2.0653L = 2r_{Au}\frac{1.4013}{1.1135} + 3r_{Au} = 7.9420$ Å

D_c / nm	D_m / nm	D_i / nm	N_v	N_c	N_m	N_i
1.717	1.674	[3] 1.659	139.2	156.0	144.4	140.6
		[4] 1.629				133.1
		[5] 1.588				123.4

Truncated Icosahedron
Cluster 135
Surface 80
Icosahedron 55

$R_c = \frac{\sqrt{58+18\sqrt{5}}}{4} L = 2.4780L = 6r_{Au}\frac{0.8090}{0.9511} + r_{Au} = 8.7891$ Å

D_c / nm	D_m / nm	D_i / nm	N_v	N_c	N_m	N_i
1.758	1.722	[5] 1.651	145.1	167.3	157.2	138.6
		[6] 1.608				128.1

Icosidodecahedron
Cluster 145
Surface 90
Icosahedron 55

[5]: $R_{in} = \sqrt{\frac{5+2\sqrt{5}}{5}} L = 1.3764L = 2r_{Au}\frac{1.4013}{1.1135} + 3r_{Au} = 7.9420$ Å

D_c / nm	D_m / nm	D_i / nm	N_v	N_c	N_m	N_i
1.867	1.776	[3] 1.744	156.4	200.5	172.5	163.5
		[5] 1.588				123.4

Icosahedron
Cluster 147
Surface 92
Icosahedron 55

$R_c = \frac{\sqrt{10+2\sqrt{5}}}{4} L = 0.9511L = 7r_{Au} = 10.08$ Å

D_c / nm	D_m / nm	D_i / nm	N_v	N_c	N_m	N_i
2.016	1.715	1.502	152.8	252.4	155.3	126.6

Dodecahedron
Cluster 165
Surface 110
Icosahedron 55

$R_i = \frac{\sqrt{10(25+11\sqrt{5})}}{20} L = 1.1135L = 6r_{Au} = 8.64$ Å

D_c / nm	D_m / nm	D_i / nm	N_v	N_c	N_m	N_i
2.175	2.031	1.728	210.6	316.7	258.2	158.9

G4

Truncated Dodecahedron
Cluster 195
Surface 120
Dodecahedron 75

$R_c = \frac{\sqrt{2(37+15\sqrt{5})}}{4} L = 2.9695L = 8r_{Au}\frac{0.7558}{0.9511} + r_{Au} = 10.594$ Å

D_c / nm	D_m / nm	D_i / nm	N_v	N_c	N_m	N_i
2.119	2.089	[3] 2.078	227.2	293.0	280.6	276.5
		[10] 1.783				174.6

Rhombicosidodecahedron
Cluster 207
Surface 72
Truncated Icosahedron 135

$R_c = \frac{\sqrt{11+4\sqrt{5}}}{2} L = 2.2330L = 8r_{Au}\frac{0.7558}{0.9511} + r_{Au} = 10.594$ Å

D_c / nm	D_m / nm	D_i / nm	N_v	N_c	N_m	N_i
2.119	2.065	[3] 2.047	261.5	293.0	271.2	264.1
		[4] 2.010				250.0
		[5] 1.960				231.8

tables for a given nanoparticle sample. Several examples can be found in the ESM (Section S5). Equipped with TEM images (even better high-resolution TEM images or TEM tomography data) that should allow the experimentalist to determine the shape(s) or closest match to one of the regular polyhedra, Archimedean icosahedra, Archimedean cubes, Ino's or Marks' decahedra, the following steps

Table 4 continued

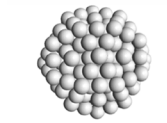

Icosidodecahedron
Cluster 237
Surface 102
Truncated Icosahedron 135

[3]: $R_{in} = \sqrt{\frac{7+3\sqrt{5}}{6}} = 1.5115L = 8r_{Au}\frac{0.7558}{0.9511} + r_{Au} = 10.594\text{Å}$

D_c / nm	D_m / nm	D_i / nm	N_v	N_c	N_m	N_i
2.268	2.157	[3] 2.119	280.3	359.4	309.2	293.0
		[5] 1.930				221.3

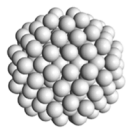

Sub-Rhombicosidodecahedron
Cluster 267
Surface 120
Icosahedron 147

[5]: $R_i = \frac{3\sqrt{5(5+2\sqrt{5})}}{10} = 2.0653L = 7r_{Au} = 10.08\text{ Å}$

D_c / nm	D_m / nm	D_i / nm	N_v	N_c	N_m	N_i
2.182	2.126	[3] 2.107	285.4	319.8	296.0	288.3
		[4] 2.069				272.9
		[5] 2.018				253.0

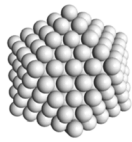

Icosahedron
Cluster 309
Surface 162
Icosahedron 147

$R_c = \frac{\sqrt{10+2\sqrt{5}}}{4}L = 0.9511L = 9r_{Au} = 12.96\text{ Å}$

D_c / nm	D_m / nm	D_i / nm	N_v	N_c	N_m	N_i
2.592	2.205	2.060	324.7	536.4	330.1	269.2

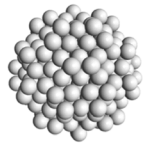

Sub-Truncated Icosahedron
Cluster 327
Surface 180
Icosahedron 147

[5]: $R_i = \frac{\sqrt{10(125+41\sqrt{5})}}{20} = 2.3274L = 8r_{Au} = 11.52\text{ Å}$

D_c / nm	D_m / nm	D_i / nm	N_v	N_c	N_m	N_i
2.453	2.403	[5] 2.304	394.4	454.7	427.2	376.7
		[6] 2.244				348.2

G5

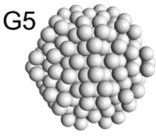

Truncated Dodecahedron
Cluster 357
Surface 120
Icosidodecahedron 237

[3]: $R_i = \frac{9\sqrt{3}+5\sqrt{15}}{12} = 2.9128L = 10r_{Au}\frac{0.7558}{0.9511} + r_{Au} = 12.883\text{ Å}$

D_c / nm	D_m / nm	D_i / nm	N_v	N_c	N_m	N_i
2.627	2.589	[3] 2.577	432.8	558.2	534.7	526.9
		[10] 2.211				332.7

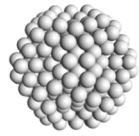

Sub-Rhombicosidodecahedron
Cluster 387
Surface 120
Sub-Rhombicosidodecahedron 267

[5]: $R_i = \frac{3\sqrt{5(5+2\sqrt{5})}}{10} = 2.0653L = 8r_{Au} = 11.52\text{ Å}$

D_c / nm	D_m / nm	D_i / nm	N_v	N_c	N_m	N_i
2.493	2.430	[3] 2.409	426.0	477.4	441.9	430.3
		[4] 2.365				407.3
		[5] 2.306				377.7

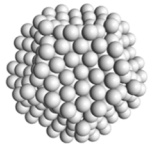

Truncated Dodecahedron
Cluster 417
Surface 150
Rhombicosidodecahedron 267

[10]: $R_i = \frac{\sqrt{2(25+11\sqrt{5})}}{4}L = 2.499L = 8r_{Au} = 11.52\text{ Å}$

D_c / nm	D_m / nm	D_i / nm	N_v	N_c	N_m	N_i
2.738	2.699	[3] 2.686	490.0	632.0	605.4	596.5
		[10] 2.304				376.7

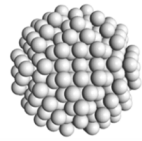

Sub-Rhombicosidodecahedron
Cluster 429
Surface 132
Sub-Icosahedron 297

[3]: $R_i = \frac{3\sqrt{3}+2\sqrt{15}}{6} = 2.1571L = 10r_{Au}\frac{0.7558}{0.9511} + r_{Au} = 12.883\text{ Å}$

D_c / nm	D_m / nm	D_i / nm	N_v	N_c	N_m	N_i
2.667	2.600	[3] 2.577	521.6	584.5	541.1	526.9
		[4] 2.530				498.7
		[5] 2.467				462.4

should lead to a close match between real and calculated core composition (a simplified flowchart of this procedure is shown in Fig. 11):

1. Zoom into the TEM image showing isolated, non-aggregated gold nanoparticles as much as possible without sacrificing (shape) resolution,
2. Using your imaging software (with analytical capabilities) measure the nanoparticle shape's features such as the various circumscribed, mid-scribed, or inscribed diameters (or radii),
3. Find the closest match in all provided tables (if the particular size is not listed, use the equations provided in Tables 2, 4, and 5), focusing

Table 4 continued

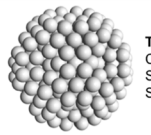

Truncated Icosidodecahedron
Cluster 437
Surface 140
Sub-Icosahedron 297

[6]: $R_i = \frac{2\sqrt{3}+\sqrt{15}}{2} = 3.6685L = 10r_{Au}\frac{0.7558}{0.9511} + r_{Au} = 12.883$ Å

D_c / nm	D_m / nm	D_i / nm	N_v	N_c	N_m	N_i
2.671	2.647	[4] 2.624	526.9	586.7	571.5	556.5
		[6] 2.577				526.9
		[12] 2.417				434.8

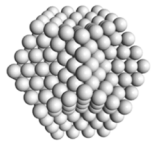

Dodecahedron
Cluster 437
Surface 170
Sub-Rhombicosidodecahedron267

$R_i = \frac{\sqrt{10(25+11\sqrt{5})}}{20}L = 1.1135L = 2r_{Au}\frac{1.4013}{1.1135} + 7r_{Au} = 12.262$ Å

D_c / nm	D_m / nm	D_i / nm	N_v	N_c	N_m	N_i
3.086	2.883	2.452	602.0	905.4	738.0	454.3

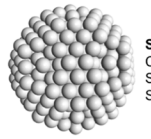

Sub-Truncated Icosahedron
Cluster 489
Surface 192
Sub-Icosahedron 297

$R_c = \frac{\sqrt{58+18\sqrt{5}}}{4}L = 2.4780L = 10r_{Au}\frac{0.8090}{0.9511} + r_{Au} = 13.689$ Å

D_c / nm	D_m / nm	D_i / nm	N_v	N_c	N_m	N_i
2.738	2.681	[5] 2.571	548.2	632.0	593.8	523.6
		[6] 2.505				484.0

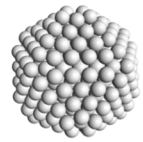

Sub-Icosahedron
Cluster 509
Surface 200
Icosahedron 309

$R_c = \frac{\sqrt{10+2\sqrt{5}}}{4}L = 0.9511L = 2r_{Au}\frac{R_c}{R_i} + 9r_{Au} = 15.142$

D_c / nm	D_m / nm	D_i / nm	N_v	N_c	N_m	N_i
3.028	2.576	2.407	517.9	855.4	526.4	429.3

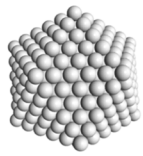

Icosahedron
Cluster 561
Surface 252
Icosahedron 309

$R_c = \frac{\sqrt{10+2\sqrt{5}}}{4}L = 0.9511L = 11r_{Au} = 15.84$

D_c / nm	D_m / nm	D_i / nm	N_v	N_c	N_m	N_i
3.168	2.695	2.517	592.9	979.3	602.7	491.4

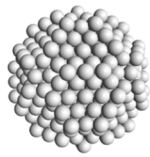

Sub-Truncated Icosahedron
Cluster 599
Surface 290
Icosahedron 309

[5]: $R_i = \frac{\sqrt{10(125+41\sqrt{5})}}{20} = 2.3274L = 2r_{Au}\frac{R_c}{R_i} + 8r_{Au} = 13.702$

D_c / nm	D_m / nm	D_i / nm	N_v	N_c	N_m	N_i
2.918	2.858	[5] 2.740	663.6	765.0	718.9	633.9
		[6] 2.670				585.9

G6

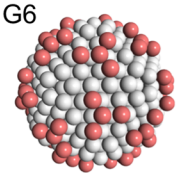

Snub Dodecahedron (enantiomer)
Cluster 629
Surface 200
Sub-Rhombicosidodecahedron 429

[3]: $R_i = \frac{\phi\xi\sqrt{3[\xi(\xi+\phi)+1]}}{6} = 2.0771L$
$= 10r_{Au}\frac{0.7558}{0.9511} + r_{Au} = 15.171$ Å

D_c / nm	D_m / nm	D_i / nm	N_v	N_c	N_m	N_i
3.149	3.064	[3] 3.034	862.5	962.2	885.7	860.6
		[5] 2.894				746.5

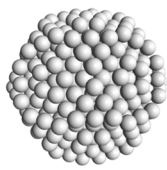

Truncated Dodecahedron
Cluster 669
Surface 240
Sub-Rhombicosidodecahedron 429

[3]: $R_i = \frac{9\sqrt{3}+5\sqrt{15}}{12} = 2.9128L$
$= 10r_{Au}\frac{0.7558}{0.9511} + r_{Au} = 15.171$ Å

D_c / nm	D_m / nm	D_i / nm	N_v	N_c	N_m	N_i
3.093	3.049	[3] 3.034	706.9	911.7	873.2	860.5
		[10] 2.603				543.4

particularly on those matching most closely the specific shape(s) visible in your TEM images (if you see a specific polygonal faces, consider the values in the square brackets for the specific polygon),

4. Once this search is narrowed to the closest match, compare the N_x/N values, with the lowest number giving the best match (N_x stands for: N_{ve}, N_c, N_m, N_i, or N_e or N_v which is the number of gold atoms calculated from the volume of a polyhedron with

Table 4 continued

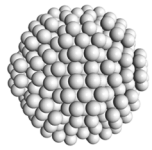

Truncated Icosidodecahedron
Cluster 689
Surface 260
Sub-Rhombicosidodecahedron 429

$[4]: R_i = \frac{3+2\sqrt{5}}{2} = 3.7361L = 10r_{Au}\frac{0.7558}{0.9511} + r_{Au} = 15.171\text{Å}$

D_c / nm	D_m / nm	D_i / nm	N_v	N_c	N_m	N_i
3.064	3.037	[4] 3.010	795.3	885.6	862.7	840.1
		[6] 2.956				795.3
		[12] 2.772				656.3

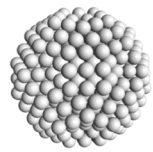

Rhombicosidodecahedron
Cluster 789
Surface 360
Sub-Rhombicosidodecahedron 429

$[5]: R_i = \frac{3\sqrt{5(5+2\sqrt{5})}}{10} = 2.0653L = 10r_{Au} = 14.4\text{ Å}$

D_c / nm	D_m / nm	D_i / nm	N_v	N_c	N_m	N_i
3.114	3.035	[3] 3.008	829.8	929.9	860.9	838.3
		[4] 2.953				793.5
		[5] 2.880				735.7

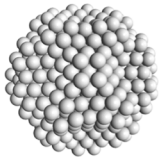

Sub-Truncated Icosidodecahedron
Cluster 839
Surface 402
Truncated Icosidodecahedron 437

$[12]: R_i = \frac{\sqrt{5(5+2\sqrt{5})}}{2} = 3.4410L = 10r_{Au} = 14.4\text{ Å}$

D_c / nm	D_m / nm	D_i / nm	N_v	N_c	N_m	N_i
3.182	3.155	[4] 3.127	891.5	992.8	967.1	941.7
		[6] 3.070				891.5
		[12] 2.880				735.7

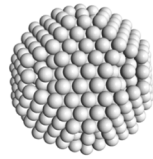

Truncated Icosahedron
Cluster 851
Surface 302
Sub-Icosahedron 549

$R_c = \frac{\sqrt{58+18\sqrt{5}}}{4}L = 2.4780L$
$= 12r_{Au}\frac{0.8090}{0.9511} + r_{Au} = 16.138\text{ Å}$

D_c / nm	D_m / nm	D_i / nm	N_v	N_c	N_m	N_i
3.228	3.161	[5] 3.031	898.4	1034	973.1	858.1
		[6] 2.953				793.2

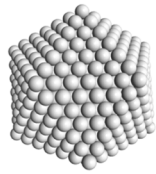

Icosahedron
Cluster 923
Surface 362
Icosahedron 561

$R_c = \frac{\sqrt{10+2\sqrt{5}}}{4}L = 0.9511L = 13r_{Au} = 18.72\text{ Å}$

D_c / nm	D_m / nm	D_i / nm	N_v	N_c	N_m	N_i
3.744	3.185	2.975	978.7	1616	994.8	811.1

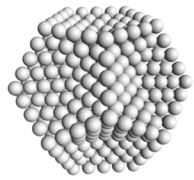

Dodecahedron
Cluster 1019
Surface 570
Truncated Icosidodecahedron 449

$R_i = \frac{\sqrt{10(25+11\sqrt{5})}}{20}L = 1.1135L = 12r_{Au} = 17.28\text{ Å}$

D_c / nm	D_m / nm	D_i / nm	N_v	N_c	N_m	N_i
4.349	4.063	3.456	1685	2534	2066	1271

The parameters and equations used are shown for each cluster. L is the edge length of the polyhedron, D_c, D_m, and D_i are the circumscribed, midscribed, and inscribed diameter (R_c is the circumscribed radius), N_v, N_c, N_m, and N_i are the number of gold atoms calculated from the volume of a polyhedron, the volume of a sphere with circumscribed diameter, the volume of a sphere with midscribed diameter, and the volume of a sphere with inscribed diameter, respectively. Numbers in square brackets for the inscribed diameter D_i or radius R_i denote faces of the Archimedean icosahedra, e.g., [3] for triangle, [5] for pentagon

the radius of an edge-scribed sphere, from a volume of a sphere with circumscribed diameter, from a volume of a sphere with midscribed diameter, from a volume of a sphere with inscribed diameter, from the volume of an elliptically shaped particle, or the volume of a given regular polyhedron, respectively),

5. The closest match between shape and the lowest number of N_x/N should give the nearest composition for the gold nanoparticle (nanocluster) core composition, and finally,
6. Use this number (n) for the Au_n particle (or numbers if multimodal size distribution is observed), compare to the quasi-spherical model (Eq. 1) to see discrepancy, and elucidate full composition including ligand shell (number of thiolates) using methods including, but not limited to NMR, elemental analysis and TGA. Consider arguments of ligand density as described in the previous section.

In Figs. 12, 13, and 14, we also provide nanocluster generation trees for decahedra, Archimedean icosahedra, and Archimedean cubes, which should help understand connections between clusters and core structures as well as facilitate making the most suitable choices when analyzing TEM images.

Table 5 List of generations (G1 to G6) of Archimedean cubes (number of atoms in cluster, on the surface, parent (inner) cluster, height, and width

G1

Cuboctahedron 13
Cluster 13
Surface 12

[4]: $R_i = \frac{\sqrt{2}}{2}L = 0.7071L = (\sqrt{2}+1)r_{Au} = 3.4765$ Å

D_c / nm	D_m / nm	D_i / nm	N_v	N_c	N_m	N_i
0.983	0.852	[3] 0.803	16.5	29.3	19.0	15.9
		[4] 0.695				10.4

G2

Truncated Octahedron 38
Cluster 38
Surface 32
Octahedron 6

[4]: $R_i = \sqrt{2}L = 1.4142L = (2\sqrt{2}+1)r_{Au} = 5.5129$ Å

D_c / nm	D_m / nm	D_i / nm	N_v	N_c	N_m	N_i
1.233	1.169	[4] 1.103	39.4	57.7	49.3	41.3
		[6] 0.955				26.8

Rhombicuboctahedron 43
Cluster 43
Surface 30
Cuboctahedron 13

[4]: $R_i = \frac{1+\sqrt{2}}{2}L = 1.2071L = (2\sqrt{2}+1)r_{Au} = 5.5129$ Å

D_c / nm	D_m / nm	D_i / nm	N_v	N_c	N_m	N_i
1.278	1.193	[3] 1.164	48.8	64.3	52.4	48.6
		[4] 1.103				41.3

Cuboctahedron 55
Cluster 55
Surface 42
Cuboctahedron 13

[4]: $R_i = \frac{\sqrt{2}}{2}L = 0.7071L = (2\sqrt{2}+1)r_{Au} = 5.5129$ Å

D_c / nm	D_m / nm	D_i / nm	N_v	N_c	N_m	N_i
1.559	1.350	[3] 1.273	65.7	116.8	75.8	63.6
		[4] 1.103				41.3

Truncated Cube 62
Cluster 62
Surface 48
Cube 14

[8]: $R_i = \frac{1+\sqrt{2}}{2}L = 1.2071L = (2\sqrt{2}+1)r_{Au} = 5.5129$ Å

D_c / nm	D_m / nm	D_i / nm	N_v	N_c	N_m	N_i
1.625	1.559	[3] 1.537	76.0	132.1	116.8	111.8
		[8] 1.103				41.3

G3

Sub-Truncated Octahedron 79
Cluster 79
Surface 60
Octahedron 19

[4]: $R_i = \sqrt{2}L = 1.4142L = (3\sqrt{2}+1)r_{Au} = 7.5494$ Å

D_c / nm	D_m / nm	D_i / nm	N_v	N_c	N_m	N_i
1.688	1.601	[4] 1.510	101.2	148.2	126.5	106.0
		[6] 1.308				68.9

Sub-Rhombicuboctahedron 92
Cluster 92
Surface 54
Truncated Octahedron 38

[4]: $R_i = \frac{1+\sqrt{2}}{2}L = 1.2071L = (3\sqrt{2}+1)r_{Au} = 7.5494$ Å

D_c / nm	D_m / nm	D_i / nm	N_v	N_c	N_m	N_i
1.750	1.634	[3] 1.594	125.4	165.0	134.5	124.7
		[4] 1.510				106.0

Snub Cube (enantiomer) 111
Cluster 111
Surface 56
Cuboctahedron 55

[4]: $R_i = \frac{1}{2}\sqrt{d^2 - \frac{L^2}{3}} = 1.1426L = (3\sqrt{2}+1)r_{Au} = 7.5494$ Å

D_c / nm	D_m / nm	D_i / nm	N_v	N_c	N_m	N_i
1.776	1.648	[3] 1.603	133.9	172.4	137.9	127.0
		[4] 1.510				106.0

Sub-Truncated Octahedron 116
Cluster 116
Surface 78
Truncated octahedron 38

[4]: $R_i = \sqrt{2}L = 1.4142L = (3\sqrt{2}+1)r_{Au} = 7.5494$ Å

D_c / nm	D_m / nm	D_i / nm	N_v	N_c	N_m	N_i
1.688	1.601	[4] 1.510	101.2	148.2	126.5	106.0
		[6] 1.308				68.9

Truncated Cuboctahedron 135
Cluster 135
Surface 80
Cuboctahedron 55

[8]: $R_i = \frac{1+2\sqrt{2}}{2} = 1.9142L = (3\sqrt{2}+1)r_{Au} = 7.5494$ Å

D_c / nm	D_m / nm	D_i / nm	N_v	N_c	N_m	N_i
1.828	1.764	[4] 1.741	150.8	188.2	169.0	162.5
		[6] 1.649				138.2
		[8] 1.510				106.0

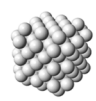

Sub-Rhombicuboctahedron 140
Cluster 140
Surface 78
Truncated cube 62

[4]: $R_i = \frac{1+\sqrt{2}}{2}L = 1.2071L = (3\sqrt{2}+1)r_{Au} = 7.5494$ Å

D_c / nm	D_m / nm	D_i / nm	N_v	N_c	N_m	N_i
1.750	1.634	[3] 1.594	125.4	165.0	134.5	124.7
		[4] 1.510				106.0

Cuboctahedron 147
Cluster 147
Surface 92
Cuboctahedron 55

[4]: $R_i = \frac{\sqrt{2}}{2}L = 0.7071L = (3\sqrt{2}+1)r_{Au} = 7.5494$ Å

D_c / nm	D_m / nm	D_i / nm	N_v	N_c	N_m	N_i
2.135	1.849	[3] 1.743	168.7	299.9	194.8	163.2
		[4] 1.510				106.0

Table 5 continued

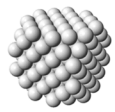

Truncated Cube 164
Cluster 164
Surface 102
Truncated cube 62

[8]: $R_i = \frac{1+\sqrt{2}}{2}L = 1.2071L = (3\sqrt{2}+1)r_{Au} = 7.5494$ Å

D_c / nm	D_m / nm	D_i / nm	N_v	N_c	N_m	N_i
2.225	2.135	[3] 2.105	195.1	339.3	299.9	287.1
		[8] 1.510				106.0

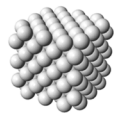

Sub-Truncated Cube 171
Cluster 171
Surface 108
Cube 63

[8]: $R_i = \frac{1+\sqrt{2}}{2}L = 1.2071L = (3\sqrt{2}+1)r_{Au} = 7.5494$ Å

D_c / nm	D_m / nm	D_i / nm	N_v	N_c	N_m	N_i
2.225	2.135	[3] 2.105	195.1	339.3	299.9	287.1
		[8] 1.510				106.0

G4

Sub-Truncated Octahedron 140
Cluster 140
Surface 96
Octahedron 44

[4]: $R_i = \sqrt{2}L = 1.4142L = (4\sqrt{2}+1)r_{Au} = 9.5859$ Å

D_c / nm	D_m / nm	D_i / nm	N_v	N_c	N_m	N_i
2.143	2.033	[4] 1.917	207.2	303.3	259.0	217.0
		[6] 1.660				141.0

Sub-Rhombicuboctahedron 165
Cluster 165
Surface 86
Sub-Truncated Octahedron 79

[4]: $R_i = \frac{1+\sqrt{2}}{2}L = 1.2071L = (4\sqrt{2}+1)r_{Au} = 9.5859$ Å

D_c / nm	D_m / nm	D_i / nm	N_v	N_c	N_m	N_i
2.222	2.075	[3] 2.024	256.7	337.9	275.3	255.3
		[4] 1.917				217.0

Truncated Octahedron 201
Cluster 201
Surface 122
Sub-Truncated Octahedron 79

[4]: $R_i = \sqrt{2}L = 1.4142L = (4\sqrt{2}+1)r_{Au} = 9.5859$ Å

D_c / nm	D_m / nm	D_i / nm	N_v	N_c	N_m	N_i
2.143	2.033	[4] 1.917	207.2	303.3	259.0	217.0
		[6] 1.660				141.0

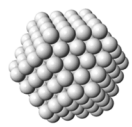

Sub-Cuboctahedron 260
Cluster 260
Surface 144
Sub-Truncated Octahedron 116

[4]: $R_i = \frac{\sqrt{2}}{2}L = 0.7071L = (4\sqrt{2}+1)r_{Au} = 9.5859$ Å

D_c / nm	D_m / nm	D_i / nm	N_v	N_c	N_m	N_i
2.711	2.348	[3] 2.214	345.4	613.9	398.7	334.2
		[4] 1.917				217.0

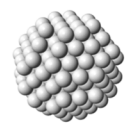

Sub-Truncated Cuboctahedron 236
Cluster 236
Surface 120
Sub-Truncated Octahedron 116

[8]: $R_i = \frac{1+2\sqrt{2}}{2} = 1.9142L = (4\sqrt{2}+1)r_{Au} = 9.5859$ Å

D_c / nm	D_m / nm	D_i / nm	N_v	N_c	N_m	N_i
2.321	2.239	[4] 2.211	308.7	385.2	345.9	332.7
		[6] 2.094				282.8
		[8] 1.917				217.0

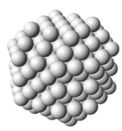

Sub-Rhombicuboctahedron 249
Cluster 249
Surface 114
Truncated Cuboctahedron 135

[4]: $R_i = \frac{1+\sqrt{2}}{2}L = 1.2071L = (4\sqrt{2}+1)r_{Au} = 9.5859$ Å

D_c / nm	D_m / nm	D_i / nm	N_v	N_c	N_m	N_i
2.222	2.075	[3] 2.024	256.7	337.9	275.3	255.3
		[4] 1.917				217.0

Sub-Snub Cube (enantiomer) 249
Cluster 249
Surface 114
Truncated Cuboctahedron 135

[4]: $R_i = \frac{1}{2}\sqrt{d^2 - \frac{L^2}{3}} = 1.1426L = (4\sqrt{2}+1)r_{Au} = 9.5859$ Å

D_c / nm	D_m / nm	D_i / nm	N_v	N_c	N_m	N_i
2.255	2.093	[3] 2.036	274.0	353.0	282.3	259.9
		[4] 1.917				217.0

Table 5 continued

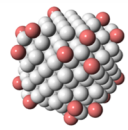

Sub-Snub Cube (enantiomer) 268
Cluster 268
Surface 128
Sub-Rhombicuboctahedron 140

[4]: $R_i = \frac{1}{2}\sqrt{d^2 - \frac{L^2}{3}} = 1.1426L = (4\sqrt{2}+1)r_{Au} = 9.5859$ Å

D_c / nm	D_m / nm	D_i / nm	N_v	N_c	N_m	N_i
2.255	2.093	[3] 2.036	274.0	353.0	282.3	259.9
		[4] 1.917				217.0

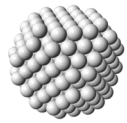

Sub-Truncated Cuboctahedron 297
Cluster 297
Surface 162
Truncated Cuboctahedron 135

[8]: $R_i = \frac{1+2\sqrt{2}}{2} = 1.9142L = (4\sqrt{2}+1)r_{Au} = 9.5859$ Å

D_c / nm	D_m / nm	D_i / nm	N_v	N_c	N_m	N_i
2.321	2.239	[4] 2.211	308.7	385.2	345.9	332.7
		[6] 2.094				282.8
		[8] 1.917				217.0

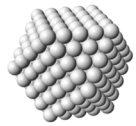

Cuboctahedron 309
Cluster 309
Surface 162
Cuboctahedron 147

[4]: $R_i = \frac{\sqrt{2}}{2}L = 0.7071L = (4\sqrt{2}+1)r_{Au} = 9.5859$ Å

D_c / nm	D_m / nm	D_i / nm	N_v	N_c	N_m	N_i
2.711	2.348	[3] 2.214	345.4	613.9	398.7	334.2
		[4] 1.917				217.0

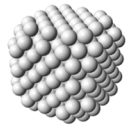

Sub-Truncated Cuboctahedron 316
Cluster 316
Surface 152
Truncated Cube 164

[8]: $R_i = \frac{1+2\sqrt{2}}{2} = 1.9142L = (4\sqrt{2}+1)r_{Au} = 9.5859$ Å

D_c / nm	D_m / nm	D_i / nm	N_v	N_c	N_m	N_i
2.321	2.239	[4] 2.211	308.7	385.2	345.9	332.7
		[6] 2.094				282.8
		[8] 1.917				217.0

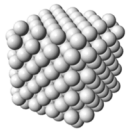

Sub-Rhombicuboctahedron 321
Cluster 321
Surface 150
Sub-Truncated Cube 171

[4]: $R_i = \frac{1+\sqrt{2}}{2}L = 1.2071L = (4\sqrt{2}+1)r_{Au} = 9.5859$ Å

D_c / nm	D_m / nm	D_i / nm	N_v	N_c	N_m	N_i
2.222	2.075	[3] 2.024	256.7	337.9	275.3	255.3
		[4] 1.917				217.0

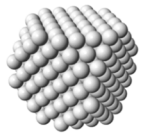

Cuboctahedron 340
Cluster 340
Surface 176
Truncated Cube 164

[4]: $R_i = \frac{\sqrt{2}}{2}L = 0.7071L = (4\sqrt{2}+1)r_{Au} = 9.5859$ Å

D_c / nm	D_m / nm	D_i / nm	N_v	N_c	N_m	N_i
2.711	2.348	[3] 2.214	345.4	613.9	398.7	334.2
		[4] 1.917				217.0

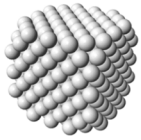

Truncated Cube 357
Cluster 357
Surface 186
Sub-Truncated Cube 171

[8]: $R_i = \frac{1+\sqrt{2}}{2}L = 1.2071L = (4\sqrt{2}+1)r_{Au} = 9.5859$ Å

D_c / nm	D_m / nm	D_i / nm	N_v	N_c	N_m	N_i
2.825	2.711	[3] 2.672	399.5	694.6	613.9	587.7
		[8] 1.917				217.0

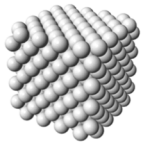

Sub-Cube 364
Cluster 364
Surface 192
Cube 172

[8]: $R_i = \frac{1}{2}L = (4\sqrt{2}+1)r_{Au} = 9.5859$ Å

D_c / nm	D_m / nm	D_i / nm	N_v	N_c	N_m	N_i
3.321	2.711	1.917	414.5	1127.8	613.9	217.0

G5

Sub-Octahedron 225
Cluster 225
Surface 140
Octahedron 85

[4]: $R_c = (5\sqrt{2}+1)r_{Au} = 11.622$ Å

D_c / nm	D_m / nm	D_i / nm	N_v	N_c	N_m	N_i
2.324	1.644	1.342	123.1	386.8	136.8	74.4

Table 5 continued

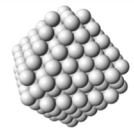

Sub-Rhombicuboctahedron 266
Cluster 266
Surface 126
Sub-Truncated Octahedron 140

[4]: $R_i = \frac{1+\sqrt{2}}{2}L = 1.2071L = (5\sqrt{2}+1)r_{Au} = 11.622$ Å

D_c / nm	D_m / nm	D_i / nm	N_v	N_c	N_m	N_i
2.694	2.516	[3] 2.454	457.5	602.2	490.5	455.1
		[4] 2.324				386.8

Sub-Truncated Octahedron 314
Cluster 314
Surface 174
Sub-Truncated Octahedron 140

[4]: $R_i = \sqrt{2}L = 1.4142L = (5\sqrt{2}+1)r_{Au} = 11.622$ Å

D_c / nm	D_m / nm	D_i / nm	N_v	N_c	N_m	N_i
2.599	2.465	[4] 2.324	369.3	540.5	461.6	386.8
		[6] 2.013				251.2

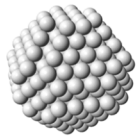

Sub-Rhombicuboctahedron 369
Cluster 369
Surface 168
Truncated Octahedron 201

[4]: $R_i = \frac{1+\sqrt{2}}{2}L = 1.2071L = (5\sqrt{2}+1)r_{Au} = 11.622$ Å

D_c / nm	D_m / nm	D_i / nm	N_v	N_c	N_m	N_i
2.694	2.516	[3] 2.454	457.5	602.2	490.5	455.1
		[4] 2.324				386.8

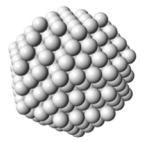

Rhombicuboctahedron 394
Cluster 394
Surface 158
Sub-Truncated Cuboctahedron 236

[4]: $R_i = \frac{1+\sqrt{2}}{2}L = 1.2071L = (5\sqrt{2}+1)r_{Au} = 11.622$ Å

D_c / nm	D_m / nm	D_i / nm	N_v	N_c	N_m	N_i
2.694	2.516	[3] 2.454	457.5	602.2	490.5	455.1
		[4] 2.324				386.8

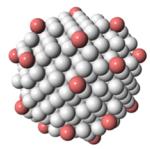

Sub-Snub Cube (enantiomer) 394
Cluster 394
Surface 158
Sub-Truncated Cuboctahedron 236

[4]: $R_i = \frac{1}{2}\sqrt{d^2 - \frac{L^2}{3}} = 1.1426L = (5\sqrt{2}+1)r_{Au} = 11.622$ Å

D_c / nm	D_m / nm	D_i / nm	N_v	N_c	N_m	N_i
2.733	2.537	[3] 2.468	488.4	629.1	503.0	463.2
		[4] 2.324				386.8

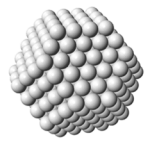

Sub-Truncated Octahedron 405
Cluster 405
Surface 204
Truncated Octahedron 201

[4]: $R_i = \sqrt{2}L = 1.4142L = (5\sqrt{2}+1)r_{Au} = 11.622$ Å

D_c / nm	D_m / nm	D_i / nm	N_v	N_c	N_m	N_i
2.599	2.465	[4] 2.324	369.3	540.5	461.6	386.8
		[6] 2.013				251.2

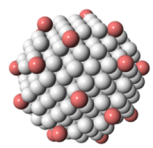

Snub Cube (enantiomer) 429
Cluster 429
Surface 132
Sub-Truncated Cuboctahedron 297

[4]: $R_i = \frac{1}{2}\sqrt{d^2 - \frac{L^2}{3}} = 1.1426L = (5\sqrt{2}+1)r_{Au} = 11.622$ Å

D_c / nm	D_m / nm	D_i / nm	N_v	N_c	N_m	N_i
2.733	2.537	[3] 2.468	488.4	629.1	503.0	463.2
		[4] 2.324				386.8

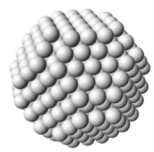

Sub-Truncated Cuboctahedron 466
Cluster 466
Surface 230
Sub-Truncated Cuboctahedron 236

[8]: $R_i = \frac{1+2\sqrt{2}}{2} = 1.9142L = (5\sqrt{2}+1)r_{Au} = 11.622$ Å

D_c / nm	D_m / nm	D_i / nm	N_v	N_c	N_m	N_i
2.814	2.715	[4] 2.680	550.2	686.5	616.5	592.9
		[6] 2.539				504.0
		[8] 2.324				386.8

Table 5 continued

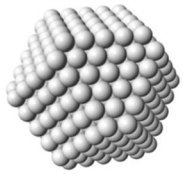

Sub-Cuboctahedron 490
Cluster 490
Surface 230
Sub-Cuboctahedron 260

[4]: $R_i = \frac{\sqrt{2}}{2}L = 0.7071L = (5\sqrt{2}+1)r_{Au} = 11.622$ Å

D_c / nm	D_m / nm	D_i / nm	N_v	N_c	N_m	N_i
3.287	2.847	[3] 2.684	615.6	1094.1	710.5	595.5
		[4] 2.324				386.8

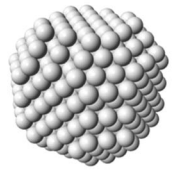

Sub-Truncated Cuboctahedron 501
Cluster 501
Surface 204
Sub-Truncated Cuboctahedron 297

[8]: $R_i = \frac{1+2\sqrt{2}}{2} = 1.9142L = (5\sqrt{2}+1)r_{Au} = 11.622$ Å

D_c / nm	D_m / nm	D_i / nm	N_v	N_c	N_m	N_i
2.814	2.715	[4] 2.680	550.2	686.5	616.5	592.9
		[6] 2.539				504.0
		[8] 2.324				386.8

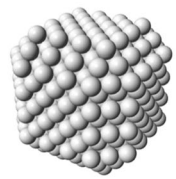

Sub-Rhombicuboctahedron 514
Cluster 514
Surface 198
Sub-Truncated Cuboctahedron 316

[4]: $R_i = \frac{1+\sqrt{2}}{2}L = 1.2071L = (5\sqrt{2}+1)r_{Au} = 11.622$ Å

D_c / nm	D_m / nm	D_i / nm	N_v	N_c	N_m	N_i
2.694	2.516	[3] 2.454	457.5	602.2	490.5	455.1
		[4] 2.324				386.8

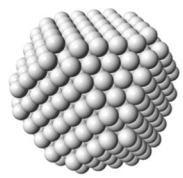

Sub-Cuboctahedron 549
Cluster 549
Surface 240
Cuboctahedron 309

[4]: $R_i = \frac{\sqrt{2}}{2}L = 0.7071L = (5\sqrt{2}+1)r_{Au} = 11.622$ Å

D_c / nm	D_m / nm	D_i / nm	N_v	N_c	N_m	N_i
3.287	2.847	[3] 2.684	615.6	1094.1	710.5	595.5
		[4] 2.324				386.8

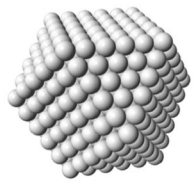

Cuboctahedron 561
Cluster 561
Surface 252
Cuboctahedron 309

[4]: $R_i = \frac{\sqrt{2}}{2}L = 0.7071L = (5\sqrt{2}+1)r_{Au} = 11.622$ Å

D_c / nm	D_m / nm	D_i / nm	N_v	N_c	N_m	N_i
3.287	2.847	[3] 2.684	615.6	1094.1	710.5	595.5
		[4] 2.324				386.8

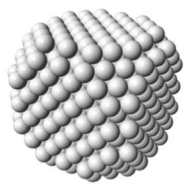

Sub-Truncated Cuboctahedron 586
Cluster 584
Surface 270
Cuboctahedron 340

[8]: $R_i = \frac{1+2\sqrt{2}}{2} = 1.9142L = (5\sqrt{2}+1)r_{Au} = 11.622$ Å

D_c / nm	D_m / nm	D_i / nm	N_v	N_c	N_m	N_i
2.814	2.715	[4] 2.680	550.2	686.5	616.5	592.9
		[6] 2.539				504.0
		[8] 2.324				386.8

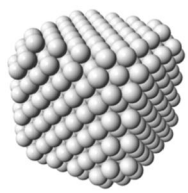

Sub-Truncated Cuboctahedron 605
Cluster 605
Surface 248
Truncated Cube 357

[8]: $R_i = \frac{1+2\sqrt{2}}{2} = 1.9142L = (5\sqrt{2}+1)r_{Au} = 11.622$ Å

D_c / nm	D_m / nm	D_i / nm	N_v	N_c	N_m	N_i
2.814	2.715	[4] 2.680	550.2	686.5	616.5	592.9
		[6] 2.539				504.0
		[8] 2.324				386.8

Table 5 continued

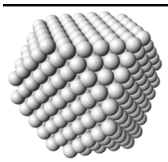

Sub-Cuboctahedron 610
Cluster 610
Surface 270
Cuboctahedron 340

[4]: $R_i = \frac{\sqrt{2}}{2}L = 0.7071L = (5\sqrt{2}+1)r_{Au} = 11.622$ Å

D_c / nm	D_m / nm	D_i / nm	N_v	N_c	N_m	N_i
3.287	2.847	[3] 2.684	615.6	1094.1	710.5	595.5
		[4] 2.324				386.8

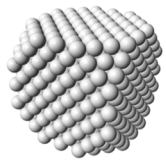

Sub-Truncated Cube 641
Cluster 641
Surface 284
Truncated Cube 357

[8]: $R_i = \frac{1+\sqrt{2}}{2}L = 1.2071L = (5\sqrt{2}+1)r_{Au} = 11.622$ Å

D_c / nm	D_m / nm	D_i / nm	N_v	N_c	N_m	N_i
3.425	3.287	[3] 3.240	711.9	1238.0	1094.0	1047.4
		[8] 2.324				386.8

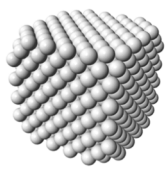

Sub-Truncated Cube 658
Cluster 658
Surface 294
Sub-Cube 364

[8]: $R_i = \frac{1+\sqrt{2}}{2}L = 1.2071L = (5\sqrt{2}+1)r_{Au} = 11.622$ Å

D_c / nm	D_m / nm	D_i / nm	N_v	N_c	N_m	N_i
3.425	3.287	[3] 3.240	711.9	1238.0	1094.0	1047.4
		[8] 2.324				386.8

G6

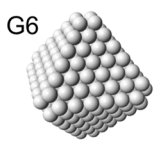

Sub-Octahedron 338
Cluster 338
Surface 192
Octahedron 146

[4]: $R_i = (6\sqrt{2}+1)r_{Au} = 13.659$ Å

D_c / nm	D_m / nm	D_i / nm	N_v	N_c	N_m	N_i
2.732	1.932	1.577	199.9	627.9	222.0	120.8

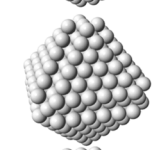

Sub-Octahedron 394
Cluster 394
Surface 169
Sub-Octahedron 225

[4]: $R_i = (6\sqrt{2}+1)r_{Au} = 13.659$ Å

D_c / nm	D_m / nm	D_i / nm	N_v	N_c	N_m	N_i
2.732	1.932	1.577	199.9	627.9	222.0	120.8

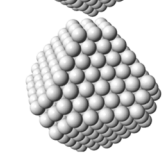

Sub-Truncated Octahedron 459
Cluster 459
Surface 234
Sub-Octahedron 225

[4]: $R_i = \sqrt{2}L = 1.4142L = (6\sqrt{2}+1)r_{Au} = 13.659$ Å

D_c / nm	D_m / nm	D_i / nm	N_v	N_c	N_m	N_i
3.054	2.898	[4] 2.732	599.4	877.5	749.3	627.9
		[6] 2.366				407.8

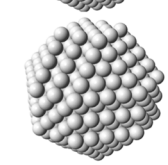

Rhombicuboctahedron 579
Cluster 579
Surface 210
Sub-Rhombicuboctahedron 369

[4]: $R_i = \frac{1+\sqrt{2}}{2}L = 1.2071L = (6\sqrt{2}+1)r_{Au} = 13.659$ Å

D_c / nm	D_m / nm	D_i / nm	N_v	N_c	N_m	N_i
3.166	2.957	[3] 2.884	742.7	977.5	796.3	738.7
		[4] 2.732				627.9

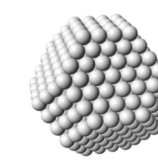

Truncated Octahedron 586
Cluster 586
Surface 272
Sub-Truncated Octahedron 314

[4]: $R_i = \sqrt{2}L = 1.4142L = (6\sqrt{2}+1)r_{Au} = 13.659$ Å

D_c / nm	D_m / nm	D_i / nm	N_v	N_c	N_m	N_i
3.054	2.898	[4] 2.732	599.4	877.5	749.3	627.9
		[6] 2.366				407.8

Table 5 continued

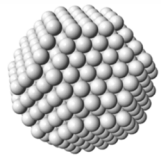

Sub-Truncated Cuboctahedron 675
Cluster 675
Surface 270
Sub-Truncated Octahedron 405

[8]: $R_i = \frac{1+2\sqrt{2}}{2} = 1.9142L = (6\sqrt{2}+1)r_{Au} = 13.659$ Å

D_c / nm	D_m / nm	D_i / nm	N_v	N_c	N_m	N_i
3.308	3.191	[4] 3.150	893.1	1114.4	1000.8	962.5
		[6] 2.984				818.2
		[8] 2.732				627.9

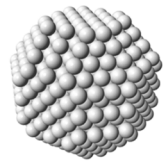

Sub-Rhombicuboctahedron
Cluster 730
Surface 264
Sub-Truncated Octahedron 466

[4]: $R_i = \frac{1+\sqrt{2}}{2}L = 1.2071L = (6\sqrt{2}+1)r_{Au} = 13.659$ Å

D_c / nm	D_m / nm	D_i / nm	N_v	N_c	N_m	N_i
3.166	2.957	[3] 2.884	742.7	977.5	796.3	738.7
		[4] 2.732				627.9

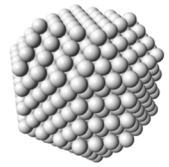

Rhombicuboctahedron 755
Cluster 755
Surface 254
Sub-Truncated Octahedron 501

[4]: $R_i = \frac{1+\sqrt{2}}{2}L = 1.2071L = (6\sqrt{2}+1)r_{Au} = 13.659$ Å

D_c / nm	D_m / nm	D_i / nm	N_v	N_c	N_m	N_i
3.166	2.957	[3] 2.884	742.7	977.5	796.3	738.7
		[4] 2.732				627.9

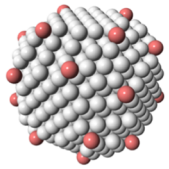

Snub Cube (enantiomer) 755
Cluster 755
Surface 254
Sub-Truncated Octahedron 501

[4]: $R_i = \frac{1}{2}\sqrt{d^2 - \frac{L^2}{3}} = 1.1426L = (6\sqrt{2}+1)r_{Au} = 13.659$ Å

D_c / nm	D_m / nm	D_i / nm	N_v	N_c	N_m	N_i
3.213	2.982	[3] 2.901	792.8	1021.2	816.6	752.0
		[4] 2.732				627.9

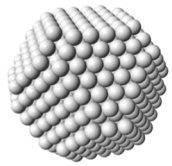

Sub-Truncated Octahedron 802
Cluster 802
Surface 312
Sub-Cuboctahedron 490

[4]: $R_i = \sqrt{2}L = 1.4142L = (6\sqrt{2}+1)r_{Au} = 13.659$ Å

D_c / nm	D_m / nm	D_i / nm	N_v	N_c	N_m	N_i
3.054	2.898	[4] 2.732	599.4	877.5	749.3	627.9
		[6] 2.366				407.8

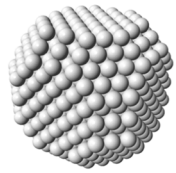

Truncated Cuboctahedron 863
Cluster 863
Surface 314
Sub-Cuboctahedron 549

[8]: $R_i = \frac{1+2\sqrt{2}}{2} = 1.9142L = (6\sqrt{2}+1)r_{Au} = 13.659$ Å

D_c / nm	D_m / nm	D_i / nm	N_v	N_c	N_m	N_i
3.308	3.191	[4] 3.150	893.1	1114.4	1000.8	962.5
		[6] 2.984				818.2
		[8] 2.732				627.9

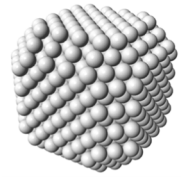

Sub-Truncated Octahedron 898
Cluster 898
Surface 312
Sub-Truncated Octahedron 586

[4]: $R_i = \sqrt{2}L = 1.4142L = (6\sqrt{2}+1)r_{Au} = 13.659$ Å

D_c / nm	D_m / nm	D_i / nm	N_v	N_c	N_m	N_i
3.054	2.898	[4] 2.732	599.4	877.5	749.3	627.9
		[6] 2.366				407.8

Table 5 continued

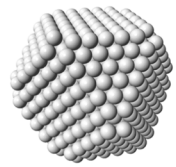

Sub-Cuboctahedron 911
Cluster 911
Surface 350
Cuboctahedron 561

[4]: $R_i = \frac{\sqrt{2}}{2}L = 0.7071L = (6\sqrt{2}+1)r_{Au} = 13.659$ Å

D_c / nm	D_m / nm	D_i / nm	N_v	N_c	N_m	N_i
3.863	3.346	[3] 3.154	999.4	1776.0	1153.5	966.8
		[4] 2.732				627.9

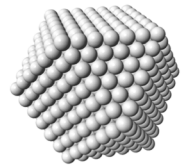

Cuboctahedron 923
Cluster 923
Surface 362
Cuboctahedron 561

[4]: $R_i = \frac{\sqrt{2}}{2}L = 0.7071L = (6\sqrt{2}+1)r_{Au} = 13.659$ Å

D_c / nm	D_m / nm	D_i / nm	N_v	N_c	N_m	N_i
3.863	3.346	[3] 3.154	999.4	1776.0	1153.5	966.8
		[4] 2.732				627.9

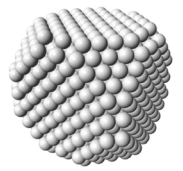

Sub-Truncated Cuboctahedron 970
Cluster 970
Surface 360
Cuboctahedron 610

[8]: $R_i = \frac{1+2\sqrt{2}}{2} = 1.9142L = (6\sqrt{2}+1)r_{Au} = 13.659$ Å

D_c / nm	D_m / nm	D_i / nm	N_v	N_c	N_m	N_i
3.308	3.191	[4] 3.150	893.1	1114.4	1000.8	962.5
		[6] 2.984				818.2
		[8] 2.732				627.9

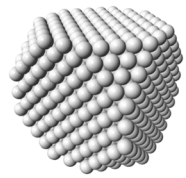

Sub-Truncated Cube 1043
Cluster 1043
Surface 402
Sub-Truncated Cube 641

[8]: $R_i = \frac{1+\sqrt{2}}{2}L = 1.2071L = (6\sqrt{2}+1)r_{Au} = 13.659$ Å

D_c / nm	D_m / nm	D_i / nm	N_v	N_c	N_m	N_i
4.026	3.863	[3] 3.808	1155.7	2009.7	1776.0	1700.3
		[8] 2.732				627.9

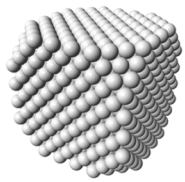

Truncated Cube
Cluster 1074
Surface 416
Sub-Truncated Cube 658

[8]: $R_i = \frac{1+\sqrt{2}}{2}L = 1.2071L = (6\sqrt{2}+1)r_{Au} = 13.659$ Å

D_c / nm	D_m / nm	D_i / nm	N_v	N_c	N_m	N_i
4.026	3.863	[3] 3.808	1155.7	2009.7	1776.0	1700.3
		[8] 2.732				627.9

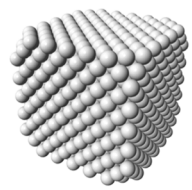

Sub-Truncated Cube
Cluster 1091
Surface 426
Cube 665

[8]: $R_i = \frac{1+\sqrt{2}}{2}L = 1.2071L = (6\sqrt{2}+1)r_{Au} = 13.659$ Å

D_c / nm	D_m / nm	D_i / nm	N_v	N_c	N_m	N_i
4.026	3.863	[3] 3.808	1155.7	2009.7	1776.0	1700.3
		[8] 2.732				627.9

The parameters and equations used are shown for each cluster. L is the edge length of the polyhedron, D_c, D_m, and D_i are the circumscribed, midscribed, and inscribed diameter (R_c is the circumscribed radius), N_v, N_c, N_m, and N_i are the number of gold atoms calculated from the volume of a polyhedron, the volume of a sphere with circumscribed diameter, the volume of a sphere with midscribed diameter, and the volume of a sphere with inscribed diameter, respectively. Numbers in square brackets for the inscribed diameter D_i or radius R_i denote faces of polygons, e.g., [3] for triangle, [5] for pentagon

Table 6 Core structures of chiral gold nanoparticles

Chiral gold nanoparticle	Core		References
	Number of core atoms	Structure	
$Au_{15}(S–CH_3)_{13}$	4	Regular tetrahedron[#]	Tlahuice-Flores et al. (2013b)
$Au_{18}(S–C_6H_{11})_{14}$	8	Continuous two octahedron	Pelayo et al. (2015)
Au_{20}(S–Ph-*t*-Bu)$_{16}$	7	Coupled two tetrahedron	Pelayo et al. (2015)
$Au_{20}(E\text{-}R_1)^a_{16}$	8	Continuous three tetrahedron	Pei et al. (2009), Takagi et al. (2015)
$Au_{20}(PP_3)_4C_{14}$	20	Icosahedron + 7 atoms	Pelayo et al. (2015)
$[Au_{20}(PPhpy_2)_{10}Cl_4]Cl_2$	20	Snub cube like	Pelayo et al. (2015)
$Au_{23}(S–C_6H_{11})_{16}$	13	Regular cuboctahedron[#]	Pelayo et al. (2015)
$Au_{24}(E–R_1)^a_{20}$	8	Continuous three tetrahedron	Pei et al. (2009); Takagi et al. (2015)
Au_{24}(S–CH_2Ph-*t*-Bu)$_{20}$	8	Cube + two tetrahedron	Pelayo et al. (2015)
Au_{24}(S-adamantane)$_{16}$	13	Regular cuboctahedron[#]	Pelayo et al. (2015)
$[Au_{25}(S–CH_2CH_2Ph)_{18}]^-$	13	Regular icosahedron[#]	Pelayo et al. (2015)
Au_{28}(S-Ph-*t*-Bu)$_{20}$	20	Continuous two icosahedron	Pelayo et al. (2015)
Au_{30}S(S-*t*-Bu)$_{18}$	20	Continuous two cuboctahedron	Pelayo et al. (2015)
Au_{36}(S–Bu)$_{24}$	28	Icosahedron + 15 atoms	Pelayo et al. (2015)
Au_{36}(S–CH_2Ph-*t*-Bu)$_8Cl_{20}$	14	Decahedron with defects	Pelayo et al. (2015)
$Au_{38}(PET)_{24}$	23	Continuous two icosahedron	Pelayo et al. (2015)
$Au_{38}(PET)_{24}$	23	Icosahedron + dodecahedron	Pelayo et al. (2015)
$Au_{38}(S–CH_2CH_2Ph)_{24}$	24	Coupled two icosahedrons	Dolamic et al. (2012)
$Au_{38}(S–R_2)^b_{24}$	24	Coupled two icosahedrons	Dolamic et al. (2012)
Au_{40}(*o*-MBT)$_{24}$	25	Rhombicuboctahedron + some atoms	Pelayo et al. (2015)
$Au_{40}(S–CH_3)_{24}$	26	Coupled two icosahedrons	Pelayo et al. (2015)
$Au_{44}(SCH_3)_{28}$	26	Decahedron + some atoms	Pelayo et al. (2015)
Au_{52}(S–Ph-*t*-Bu)$_{32}$	32	Marks' decahedron with defects	Pelayo et al. (2015)
$Au_{68}(SH)_{34}$	15	Cuboctahedron + some atoms	Pelayo et al. (2015)
Au_{68}(3-MBA)$_{50}$	50	Icosidodecahedron with defect	Pelayo et al. (2015)
Au_{102}(*p*-MBA)$_{44}$	79	Rhombicosidodecahedron with defects or Ino's, Marks' decahedron with defects	Levi-Kalisman et al. (2011), Pelayo et al. (2015)
Au_{130}(*p*-MBT)$_{50}$	105	Marks' decahedron with defects	Pelayo et al. (2015), Zeng et al. (2015)
Au_{133}(S–Ph-*p*–*t*-Bu)$_{52}$	107	Rhombicosidodecahedron with defects	Pelayo et al. (2015), Zeng et al. (2015)
$Au_{144}(S–R_3)^c_{60}$	114	Rhombicosidodecahedron with defects	Pelayo et al. (2015), Qian and Jin (2009), Weissker et al. (2014)
$Au_{144}Cl_{60}$	114	Rhombicosidodecahedron with defects	Pelayo et al. (2015), Tlahuice-Flores et al. (2013a)

[a] E = Se, S; R_1 = Ph, CH_3

[b] R_2 = CH_3, C_6H_{13}, $C_{12}H_{25}$

[c] R_3 = CH_3, CH_2CH_2Ph

[#] Gold nanoparticles with regular polyhedra cores

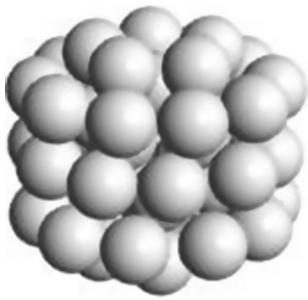

Fig. 10 Model for the chiral Au_{53} cluster

Discussion

As one can appreciate, the approach pursued here, culminating in the presented nanoparticle tables, equations, and models, solely relies on geometrical considerations not precise electronic and atomic structural information, which are only accessible for well-defined clusters whose structure was solved by X-ray diffraction (Chen et al. 2015; Jadzinsky et al. 2007; Zeng et al. 2014, 2015) or high-resolution single-particle TEM (Azubel et al. 2014) (aberration-corrected TEM, vide supra). Numerous groups have made significant and important progress in applying density functional theory and other numerical as well as computational approaches to determine gold nanoparticle sizes, structures, and energetics (Barnard 2010; Barnard and Chen 2011; Barnard and Curtiss 2006; Barnard et al. 2009; McKenna 2009; Negishi et al. 2015) and focus increasingly on the very challenging task of elucidating the structure of the thiolate ligand shell (Barnard 2013; Xu et al. 2015). A closer look at these modeling and simulation data on various gold nanoparticle sizes and shapes, however, reveals that the current geometrically derived data

Table 7 Examples of calculated surface areas for selected nanoparticle cores and corresponding densities of thiolate ligands (from Eq. 6 and Table 2)

Gold nanoparticle	Core	S_c/Å^2	N_L	ρ_L/Å^2
Au_{24}(S-adamantane)$_{16}$	Cuboctahedron 13 [12 + 1]	228.8	11[a]	20.8
$[Au_{25}(S–CH_2CH_2Ph)_{18}]^-$	Icosahedron 13 [12 + 1]	178.7	12[a]	14.89
$Au_{54}(S–C_{18}H_{37})_{30}$ $Au_{55}(S–C_{18}H_{37})_{31}$	Ino's decahedron 39 - 2 (m, n, p = 3, 2, 1)	327.9	18[a]	18.2
$Au_{144}(S–CH_3)_{60}$	Rhombicosidodecahedron 114 [60 + 54]	877.0	60	14.6
$Au_{187}(S–C_{12}H_{25})_{68}$	Truncated cuboctahedron 135 [80 + 55]	960.6	68	14.1
	Cuboctahedron 147 [92 + 55]	1079		15.9
	Marks' decahedron 153 (m, n, p = 2, 5, 2)	1127		16.6
$Au_{333}(S-CH_2CH_2Ph)_{79}$	Sub-truncated octahedron 314 [198 + 116]	1809	79	22.9
	Cuboctahedron 309 [162 + 147]	1739		22.0
	Sub-truncated cuboctahedron 297 [162 + 135]	1549		19.6
	Ino's decahedron 309 (m, n, p = 5, 5, 1)	1256		15.9
	Marks' decahedron 318 (m, n, p = 4, 3, 2)	1161		14.1

[a] The number of ligands on the core surface is lower than the total number of ligands on the gold nanoparticle, because gold nanoparticles are formed by –S–Au–S–Au–S–"staple" motifs. In this case, the number of gold atom in the shell is substituted for the number of ligands on the core surface (N_L)

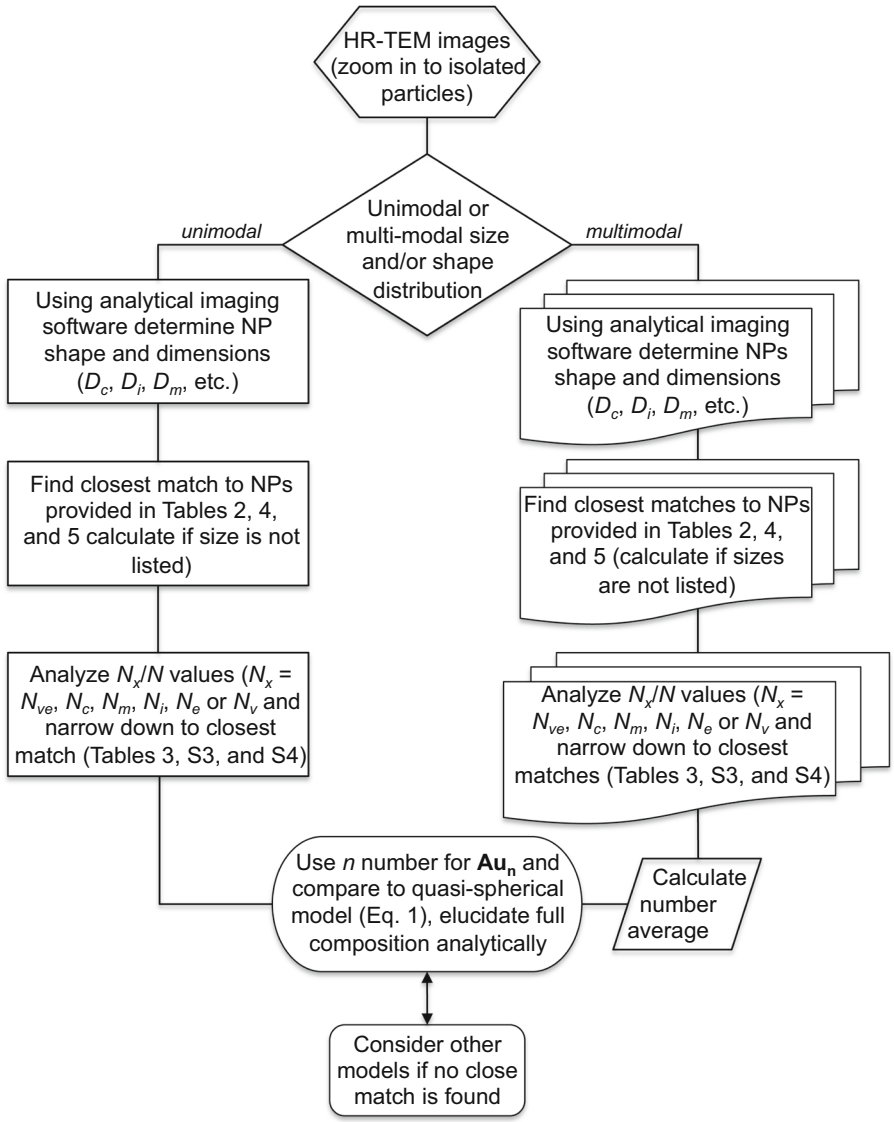

Fig. 11 Flowchart diagram of the procedure to obtain the closest match in gold nanoparticle core composition from available experimental values obtained by TEM (ideally HR-TEM or TEM tomography) image analysis

tables and models capture these and that the implementation of both approaches endows experimental scientists with a powerful tool for the elucidation of nanoparticle composition. In addition, the geometrical models can much faster survey a greater number of nanoparticles and nanoclusters (including nanoparticles with larger diameters and many more gold atoms in the core) much faster. Practically speaking, the presented equations and tables are easily adjustable (via the radius of the metal atom) for the determination of the composition of other metal nanoparticles with fcc lattices (Pd, Pt, Ni (Lin et al. 2011) as well as coinage metals Ag, Cu); perhaps even alloy-type metal nanoparticles if elemental

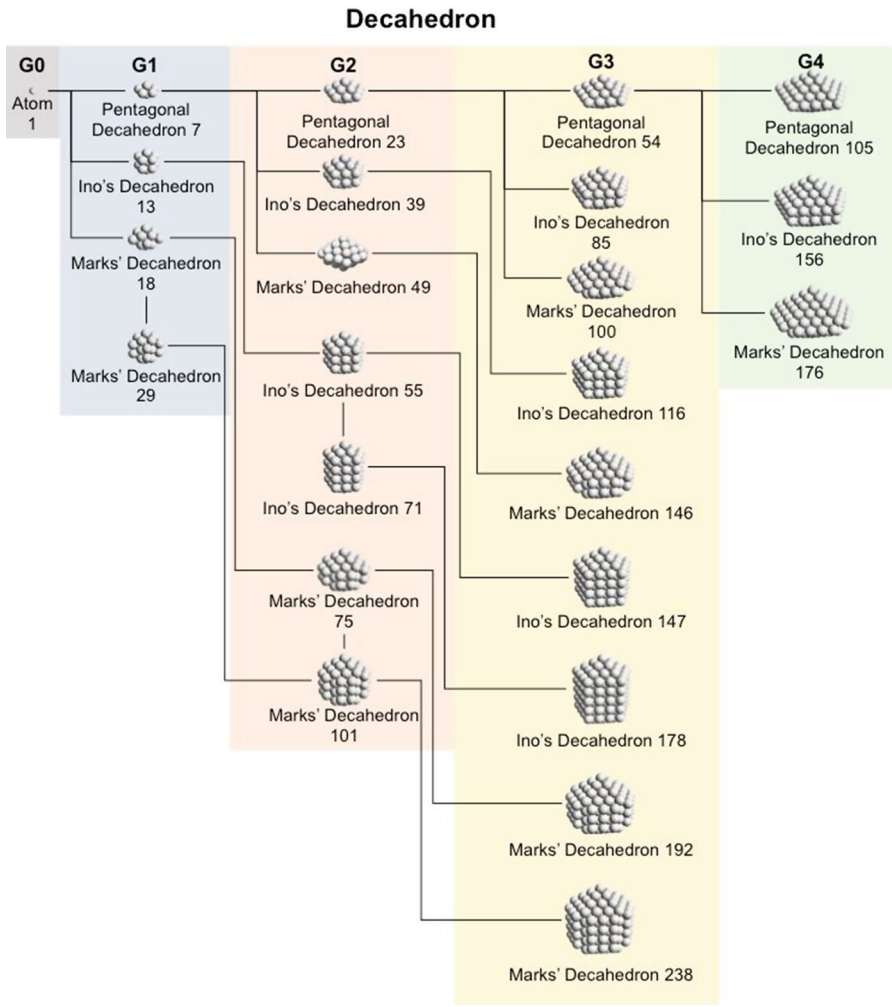

Fig. 12 Generation tree for pentagonal decahedra as well as Ino's and Marks' decahedra

composition is determined upfront. The predicted sequences of preferred shapes by Guisbiers et al. should here be tremendously helpful (Guisbiers et al. 2014). Of the 130 + clusters included in the current tables and models, several have not been experimentally observed for gold nanoparticles as of yet, and specific shapes observed for other transition metals are not included (e.g., tetrahedral for Pd nanoparticles (Barnard 2012)). Expansion to other shapes is a focus of future work, and numerical and theoretical methods recently presented by Barnard et al. will be used as guide for metal nanorods (Gonzalez et al. 2013). Finally, the section on shell structures is currently limited to the most frequently used thiolates and not considering other ligand motifs such as amines or phosphines among others. Thinking about the vast number of thiolate ligands reported in the literature, steric considerations are extremely difficult to include in any model system (Burgi 2015; Hakkinen 2012), especially since more and more sophisticated

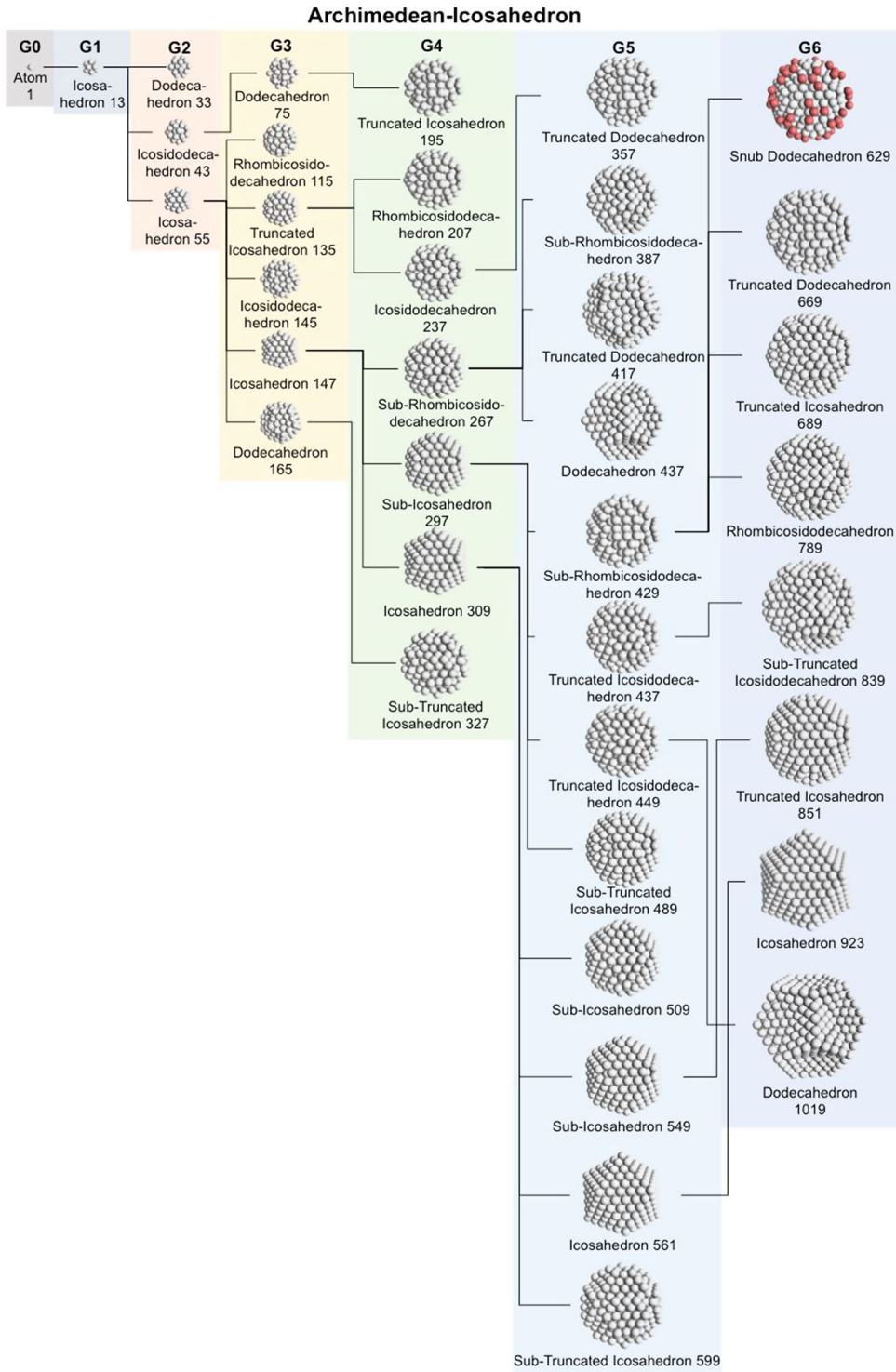

Fig. 13 Generation tree for Archimedean icosahedra

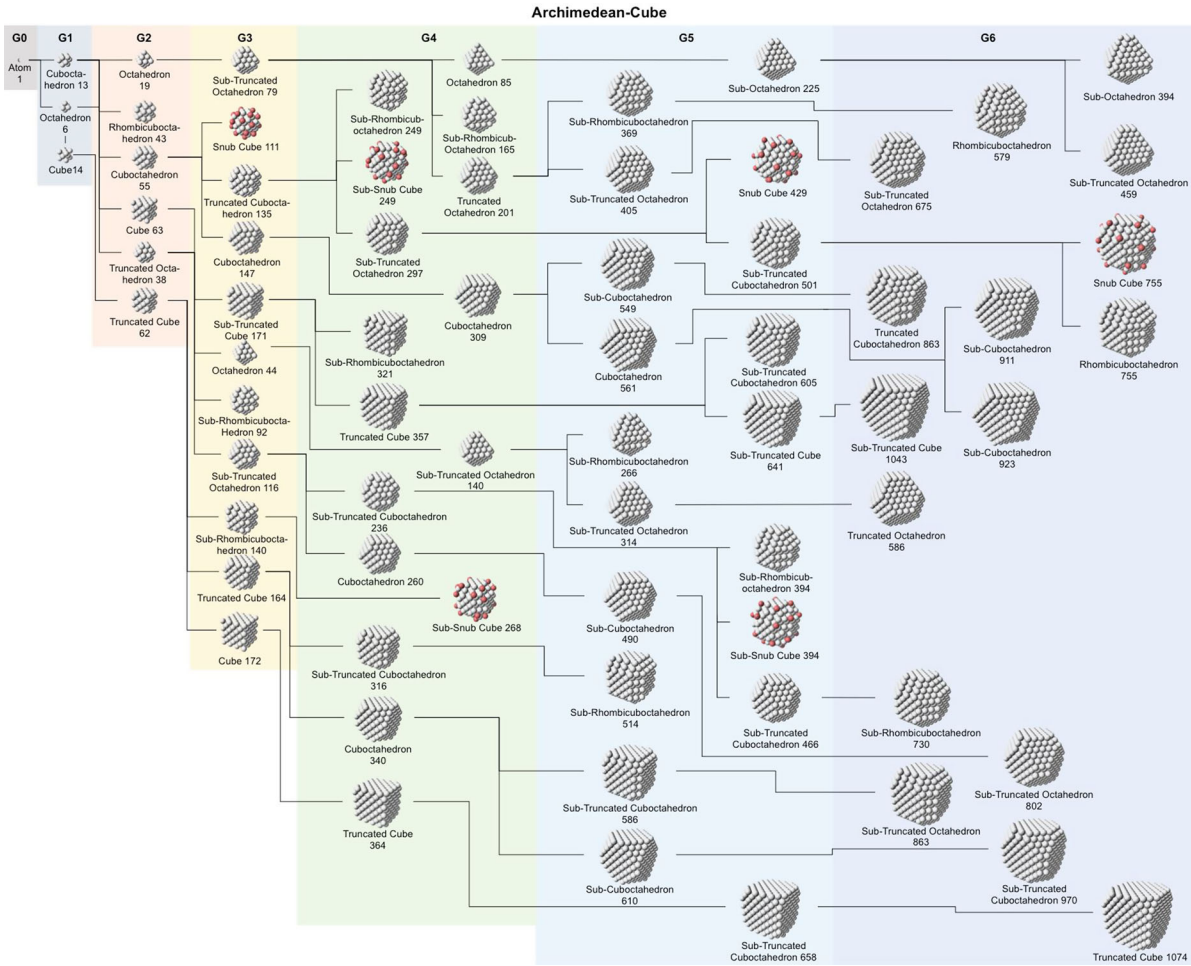

Fig. 14 Generation tree for Archimedean cubes

functions expected from gold nanoparticles require functional ligands with, for example, luminescent properties, binding capabilities to proteins, chirality, drug delivery, and many more.

Conclusions

Centered specifically around geometrical considerations, this compendium of tables, models, and equations serves as an easy-to-use, straightforward guide for experimental scientists synthesizing thiol-protected gold nanoparticles in the laboratory to assist them in calculating the nanoparticle composition based on geometric information deduced from TEM imaging and image analysis. The majority of research thrusts and applications focusing on thiol-protected metal nanoparticles do not require the precision of well-defined metal clusters, although synthetic approaches to obtain such clusters are tirelessly pursued and refined. Nevertheless, predicting and analytically confirming the composition of all other metal nanoparticles as accurately as possible is critical for fundamental and applied research alike. A nanoparticle's composition significantly affects its properties and defines its function, irrespective of its use in applications ranging from drug delivery and cancer diagnostics to metamaterials and chiral

discriminators. With the anticipated transformation of these tables, models, and equations to a web-based tool (that would also permit viewing of model clusters from various perspectives), we trust that experimental scientists will be provided with an invaluable, helpful, and expandable tool for the elucidation of metal nanoparticle compositions.

Acknowledgments This work was financially supported by the National Science Foundation (NSF, DMR-1506018), the Ohio Third Frontier (OTF) program for Ohio Research Scholars "Research Cluster on Surfaces in Advanced Materials" (T.H.), and the Japan Society for the Promotion of Science (JSPS, postdoctoral scholarship for T.M.).

References

Aillon KL, Xie Y, El-Gendy N, Berkland CJ, Forrest ML (2009) Effects of nanomaterial physicochemical properties on in vivo toxicity. Adv Drug Deliv Rev 61:457–466. doi:10.1016/j.addr.2009.03.010

Alexandridis P (2011) Gold nanoparticle synthesis, morphology control, and stabilization facilitated by functional polymers. Chem Eng Technol 34:15–28. doi:10.1002/ceat.201000335

Almeida JPM, Chen AL, Foster A, Drezek R (2011) In vivo biodistribution of nanoparticles. Nanomedicine 6:815–835. doi:10.2217/nnm.11.79

Askim JR, Mahmoudi M, Suslick KS (2013) Optical sensor arrays for chemical sensing: the optoelectronic nose. Chem Soc Rev 42:8649–8682. doi:10.1039/c3cs60179j

Azubel M et al (2014) Electron microscopy of gold nanoparticles at atomic resolution. Science 345:909–912. doi:10.1126/science.1251959

Azzazy HME, Mansour MMH, Kazmierczak SC (2006) Nanodiagnostics: a new frontier for clinical laboratory medicine. Clin Chem 52:1238–1246. doi:10.1373/clinchem.2006.066654

Baer DR, Gaspar DJ, Nachimuthu P, Techane SD, Castner DG (2010) Application of surface chemical analysis tools for characterization of nanoparticles. Anal Bioanal Chem 396:983–1002. doi:10.1007/s00216-009-3360-1

Barnard AS (2010) Modelling of nanoparticles: approaches to morphology and evolution. Rep Prog Phys 73:086502. doi:10.1088/0034-4885/73/8/086502

Barnard AS (2012) Mapping the shape and phase of palladium nanocatalysts. Catal Sci Technol 2:1485–1492. doi:10.1039/c2cy20017a

Barnard AS (2013) Modeling the impact of alkanethiol SAMs on the morphology of gold nanocrystals. Cryst Growth Des 13:5433–5441. doi:10.1021/cg401397y

Barnard AS, Chen Y (2011) Kinetic modelling of the shape-dependent evolution of faceted gold nanoparticles. J Mater Chem 21:12239–12245. doi:10.1039/c1jm11677k

Barnard AS, Curtiss LA (2006) Predicting the shape and structure of face-centered cubic gold nanocrystals smaller than 3 nm. ChemPhysChem 7:1544–1553. doi:10.1002/cphc.200600107

Barnard AS, Young NP, Kirkland AI, van Huis MA, Xu HF (2009) Nanogold: a quantitative phase map. ACS Nano 3:1431–1436. doi:10.1021/nn900220k

Ben-Moshe A, Maoz BM, Govorov AO, Markovich G (2013) Chirality and chiroptical effects in inorganic nanocrystal systems with plasmon and exciton resonances. Chem Soc Rev 42:7028–7041

Bhattacharyya S, Kudgus RA, Bhattacharya R, Mukherjee P (2011) Inorganic nanoparticles in cancer therapy. Pharm Res 28:237–259. doi:10.1007/s11095-010-0318-0

Bishop KJM, Wilmer CE, Soh S, Grzybowski BA (2009) Nanoscale forces and their uses in self-assembly. Small 5:1600–1630. doi:10.1002/smll.200900358

Boeker A, He J, Emrick T, Russell TP (2007) Self-assembly of nanoparticles at interfaces. Soft Matter 3:1231–1248. doi:10.1039/b706609k

Brust M, Walker M, Bethell D, Schiffrin DJ, Whyman R (1994) Synthesis of thiol-derivatised gold nanoparticles in a two-phase liquid–liquid system. J Chem Soc Chem Commun. doi:10.1039/C39940000801

Brust M, Fink J, Bethell D, Schiffrin DJ, Kiely C (1995) Synthesis and reactions of functionalized gold nanoparticles. J Chem Soc Chem Commun. doi:10.1039/C39950001655

Burgi T (2015) Properties of the gold-sulphur interface: from self-assembled monolayers to clusters. Nanoscale 7:15553–15567. doi:10.1039/c5nr03497c

Chen Y et al (2015) Crystal structure of barrel-shaped chiral Au130(p-MBT)50 nanocluster. J Am Chem Soc 137:10076–10079

Chikkaveeraiah BV, Bhirde AA, Morgan NY, Eden HS, Chen X (2012) Electrochemical immunosensors for detection of cancer protein biomarkers. ACS Nano 6:6546–6561. doi:10.1021/nn3023969

Crooks RM, Zhao MQ, Sun L, Chechik V, Yeung LK (2001) Dendrimer-encapsulated metal nanoparticles: synthesis, characterization, and applications to catalysis. Acc Chem Res 34:181–190. doi:10.1021/ar000110a

Dolamic I, Knoppe S, Dass A, Burgi T (2012) First enantioseparation and circular dichroism spectra of Au-38 clusters protected by achiral ligands. Nat Commun 3:798. doi:10.1038/ncomms1802

Dreaden EC, Mackey MA, Huang X, Kang B, El-Sayed MA (2011) Beating cancer in multiple ways using nanogold. Chem Soc Rev 40:3391–3404. doi:10.1039/c0cs00180e

Ganguli AK, Ganguly A, Vaidya S (2010) Microemulsion-based synthesis of nanocrystalline materials. Chem Soc Rev 39:474–485. doi:10.1039/b814613f

Gautier C, Bürgi T (2009) Chiral gold nanoparticles. ChemPhysChem 10:483–492

Gindy ME, Prud'homme RK (2009) Multifunctional nanoparticles for imaging, delivery and targeting in cancer therapy.

Expert Opin Drug Deliv 6:865–878. doi:10.1517/17425240902932908
Gonzalez AL, Noguez C, Barnard AS (2013) Mapping the structural and optical properties of anisotropic gold nanoparticles. J Mater Chem C 1:3150–3157. doi:10.1039/c3tc30313f
Gopidas KR, Whitesell JK, Fox MA (2003) Nanoparticle-cored dendrimers: synthesis and characterization. J Am Chem Soc 125:6491–6502. doi:10.1021/ja029544m
Grzelczak M, Perez-Juste J, Mulvaney P, Liz-Marzán LM (2008) Shape control in gold nanoparticle synthesis. Chem Soc Rev 37:1783–1791. doi:10.1039/b711490g
Grzelczak M, Vermant J, Furst EM, Liz-Marzán LM (2010) Directed self-assembly of nanoparticles. ACS Nano 4:3591–3605. doi:10.1021/nn100869j
Guerrero-Martínez A, Alonso-Gómez JL, Auguié B, Cid MM, Liz-Marzán LM (2011) From individual to collective chirality in metal nanoparticles. Nano Today 6:381–400
Guisbiers G, Meija-Rosales S, Khanal S, Ruiz-Zepeda F, Whetten RL, Jose-Yacaman M (2014) Gold copper nano-alloy, "Tumbaga", in the era of nano: phase diagram and segregation. Nano Lett 14:6718–6726. doi:10.1021/nl503584q
Hakkinen H (2012) The gold-sulfur interface at the nanoscale. Nat Chem 4:443–455. doi:10.1038/nchem.1352
Hegmann T, Qi H, Marx VM (2007) Nanoparticles in liquid crystals: synthesis, self-assembly, defect formation and potential applications. J Inorg Organomet Polym Mater 17:483–508. doi:10.1007/S10904-007-9140-5
Hou W, Cronin SB (2013) A review of surface plasmon resonance-enhanced photocatalysis. Adv Funct Mater 23:1612–1619. doi:10.1002/adfm.201202148
Howes PD, Chandrawati R, Stevens MM (2014) Colloidal nanoparticles as advanced biological sensors. Science 346:53. doi:10.1126/science.1247390
Jadzinsky PD, Calero G, Ackerson CJ, Bushnell DA, Kornberg RD (2007) Structure of a thiol monolayer-protected gold nanoparticle at 1.1 Å resolution. Science 318:430–433
Jain S, Hirst DG, O'Sullivan JM (2012) Gold nanoparticles as novel agents for cancer therapy British. J Radiol 85:101–113. doi:10.1259/bjr/59448833
Jiang HY, Cai WS, Shao XG (2003) New lowest energy sequence of Marks' decahedral Lennard-Jones clusters containing up to 10,000 atoms. J Phys Chem A 107:4238–4243. doi:10.1021/jp0342327
Johnston HJ, Hutchison G, Christensen FM, Peters S, Hankin S, Stone V (2010) A review of the in vivo and in vitro toxicity of silver and gold particulates: particle attributes and biological mechanisms responsible for the observed toxicity. Crit Rev Toxicol 40:328–346. doi:10.3109/10408440903453074
Kennedy LC et al (2011) A new era for cancer treatment: gold-nanoparticle-mediated thermal therapies. Small 7:169–183. doi:10.1002/smll.201000134
Khlebtsov N, Dykman L (2011) Biodistribution and toxicity of engineered gold nanoparticles: a review of in vitro and in vivo studies. Chem Soc Rev 40:1647–1671. doi:10.1039/c0cs00018c
Kim HN, Ren WX, Kim JS, Yoon J (2012) Fluorescent and colorimetric sensors for detection of lead, cadmium, and mercury ions. Chem Soc Rev 41:3210–3244. doi:10.1039/c1cs15245a
Kimura K, Sugimoto N, Sato S, Yao H, Negishi Y, Tsukuda T (2009) Size determination of gold clusters by polyacrylamide gel electrophoresis in a large cluster region. J Phys Chem C 113:14076–14082
Lal S, Clare SE, Halas NJ (2008) Nanoshell-enabled photothermal cancer therapy: impending clinical impact. Acc Chem Res 41:1842–1851. doi:10.1021/ar800150g
Leff DV, Ohara PC, Heath JR, Gelbart WM (1995) Thermodynamic control of gold nanocrystal size—experiment and theory. J Phys Chem 99:7036–7041. doi:10.1021/J100018a041
Levi-Kalisman Y, Jadzinsky PD, Kalisman N, Tsunoyama H, Tsukuda T, Bushnell DA, Kornberg RD (2011) Synthesis and characterization of Au102(p-MBA)44 nanoparticles. J Am Chem Soc 133:2976–2982
Lin C, Liu Y, Rinker S, Yan H (2006) DNA tile based self-assembly: building complex nanoarchitectures. ChemPhysChem 7:1641–1647. doi:10.1002/cphc.200600260
Lin ZZ, Chen X, Yin C, Tang H, Hu YC, Ning XJ (2011) Theoretical prediction of the growth and surface structure of Pt and Ni nanoparticles. Europhys Lett 96:66005. doi:10.1209/0295-5075/96/66005
Lohse SE, Murphy CJ (2013) The quest for shape control: a history of gold nanorod synthesis. Chem Mater 25:1250–1261. doi:10.1021/cm303708p
Lopez-Acevedo O, Tsunoyama H, Tsukuda T, Aikens CM (2010) Chirality and electronic structure of the thiolate-protected Au38 nanocluster. J Am Chem Soc 132:8210–8218
Love JC, Estroff LA, Kriebel JK, Nuzzo RG, Whitesides GM (2005) Self-assembled monolayers of thiolates on metals as a form of nanotechnology. Chem Rev 105:1103–1169. doi:10.1021/cr0300789
Lu X, Rycenga M, Skrabalak SE, Wiley B, Xia Y (2009) Chemical synthesis of novel plasmonic nanoparticles. Ann Rev Phys Chem 60:167–192. doi:10.1146/annurev.physchem.040808.090434
McKenna KP (2009) Gold nanoparticles under gas pressure. Phys Chem Chem Phys 11:4145–4151. doi:10.1039/b821408p
Mourdikoudis S, Liz-Marzán LM (2013) Oleylamine in nanoparticle synthesis. Chem Mater 25:1465–1476. doi:10.1021/cm4000476
Mulder WJM, Strijkers GJ, Van Tilborg GAF, Cormode DP, Fayad ZA, Nicolay K (2009) Nanoparticulate assemblies of amphiphiles and diagnostically active materials for multimodality imaging. Acc Chem Res 42:904–914. doi:10.1021/ar800223c
Negishi Y, Sakamoto C, Ohyama T, Tsukuda T (2012) Synthesis and the origin of the stability of thiolate-protected Au130 and Au187 clusters. J Phys Chem Lett 3:1624–1628
Negishi Y et al (2015) A critical size for emergence of nonbulk electronic and geometric structures in dodecanethiolate-protected Au clusters. J Am Chem Soc 137:1206–1212
Ofir Y, Samanta B, Rotello VM (2008) Polymer and biopolymer mediated self-assembly of gold nanoparticles. Chem Soc Rev 37:1814–1823. doi:10.1039/b712689c
Panigrahi S et al (2007) Synthesis and size-selective catalysis by supported gold nanoparticles: study on heterogeneous and

homogeneous catalytic process. J Phys Chem C 111:4596–4605. doi:10.1021/jp067554u
Pei Y, Gao Y, Shao N, Zeng XC (2009) Thiolate-protected Au-20(SR)(16) cluster: prolate Au-8 core with new [Au-3(SR)(4)] staple motif. J Am Chem Soc 131:13619–13621. doi:10.1021/ja905359b
Pelayo JJ, Whetten RL, Garzón IL (2015) Geometric quantification of chirality in ligand-protected metal clusters. J Phys Chem C 119:28666–28678
Pensa E et al (2012) The chemistry of the sulfur-gold interface: in search of a unified model. Acc Chem Res 45:1183–1192. doi:10.1021/ar200260p
Perfezou M, Turner A, Merkoci A (2012) Cancer detection using nanoparticle-based sensors. Chem Soc Rev 41:2606–2622. doi:10.1039/c1cs15134g
Pingarron JM, Yanez-Sedeno P, Gonzalez-Cortes A (2008) Gold nanoparticle-based electrochemical biosensors. Electrochim Acta 53:5848–5866. doi:10.1016/j.electacta.2008.03.005
Pyell U (2010) Characterization of nanoparticles by capillary electromigration separation techniques. Electrophoresis 31:814–831. doi:10.1002/elps.200900555
Qi H, Hegmann T (2008) Impact of nanoscale particles and carbon nanotubes on current and future generations of liquid crystal displays. J Mater Chem 18:3288–3294. doi:10.1039/B718920f
Qian HF, Jin RC (2009) Controlling nanoparticles with atomic precision: the case of Au-144(SCH2CH2Ph)(60). Nano Lett 9:4083–4087. doi:10.1021/nl902300y
Qian H, Zhu Y, Jin R (2012) Atomically precise gold nanocrystal molecules with surface plasmon resonance. Proc Natl Acad Sci USA 109:696–700
Reimers JR, Ford MJ, Halder A, Ulstrup J, Hush NS (2016) Gold surfaces and nanoparticles are protected by Au(0)–thiyl species and are destroyed when Au(I)–thiolates form. Proc Natl Acad Sci USA 113:E1424–E1433. doi:10.1073/pnas.1600472113
Rosi NL, Mirkin CA (2005) Nanostructures in biodiagnostics. Chem Rev 105:1547–1562. doi:10.1021/cr030067f
Ross MB, Mirkin CA, Schatz GC (2016) Optical properties of one-, two-, and three-dimensional arrays of plasmonic nanostructures. J Phys Chem C 120:816–830. doi:10.1021/acs.jpcc.5b10800
Sarina S, Waclawik ER, Zhu H (2013) Photocatalysis on supported gold and silver nanoparticles under ultraviolet and visible light irradiation. Green Chem 15:1814–1833. doi:10.1039/c3gc40450a
Sepulveda B, Angelome PC, Lechuga LM, Liz-Marzan LM (2009) LSPR-based nanobiosensors. Nano Today 4:244–251. doi:10.1016/j.nantod.2009.04.001
Shan J, Tenhu H (2007) Recent advances in polymer protected gold nanoparticles: synthesis, properties and applications. Chem Commun. doi:10.1039/b707740h
Shivakumar U, Mirzaei J, Feng X, Sharma A, Moreira P, Hegmann T (2011) Nanoparticles: complex and multifaceted additives for liquid crystals. Liq Cryst 38:1495–1514. doi:10.1080/02678292.2011.605477
Stamatoiu O, Mirzaei J, Feng X, Hegmann T (2012) Nanoparticles in liquid crystals and liquid crystalline nanoparticles. Top Curr Chem 318:331–393. doi:10.1007/128_2011_233
Stewart ME, Anderton CR, Thompson LB, Maria J, Gray SK, Rogers JA, Nuzzo RG (2008) Nanostructured plasmonic sensors. Chem Rev 108:494–521. doi:10.1021/cr068126n
Takagi N et al (2015) How can we understand Au8 cores and entangled ligands of selenolate- and thiolate-protected gold nanoclusters Au24(ER)20 and Au20(ER)16 (E = Se, S; R = Ph, Me)? A theoretical study. J Am Chem Soc 137:8593–8602
Tlahuice-Flores A (2015) New insight into the structure of thiolated gold clusters: a structural prediction of the Au-187(SR)(68) cluster. Phys Chem Chem Phys 17:5551–5555. doi:10.1039/c4cp05695g
Tlahuice-Flores A, Black DM, Bach SBH, Jose-Yacaman M, Whetten RL (2013a) Structure & bonding of the gold-subhalide cluster I-Au144Cl60[z]. Phys Chem Chem Phys 15:19191–19195. doi:10.1039/c3cp53902d
Tlahuice-Flores A, Jose-Yacaman M, Whetten RL (2013b) On the structure of the thiolated Au-15 cluster. Phys Chem Chem Phys 15:19557–19560. doi:10.1039/c3cp53837k
Tsunoyama R, Tsunoyama H, Pannopard P, Limtrakul J, Tsukuda T (2010) MALDI mass analysis of 11 kDa gold clusters protected by octadecanethiolate ligands. J Phys Chem C 114:16004–16009
Tweney RD, Mears RP, Spitzmüller C (2004) Replicating the practices of discovery: Michael Faraday and the interaction of gold and light. In: Gorman M, Tweney RD, Gooding D, Kincannon A (eds) Scientific and technological thinking. Lawrence Erlbaum Associates, Mahwah, NJ, pp 137–158
Walther A, Mueller AHE (2013) Janus particles: synthesis, self-assembly, physical properties, and applications. Chem Rev 113:5194–5261. doi:10.1021/cr300089t
Wang M, Thanou M (2010) Targeting nanoparticles to cancer. Pharmacol Res 62:90–99. doi:10.1016/j.phrs.2010.03.005
Wang Y, Xu J, Wang Y, Chen H (2013) Emerging chirality in nanoscience. Chem Soc Rev 42:2930–2962. doi:10.1039/c2cs35332f
Weissker HC et al (2014) Information on quantum states pervades the visible spectrum of the ubiquitous Au-144(SR)(60) gold nanocluster. Nat Commun 5:3785. doi:10.1038/ncomms4785
Wolinsky JB, Grinstaff MW (2008) Therapeutic and diagnostic applications of dendrimers for cancer treatment. Adv Drug Deliv Rev 60:1037–1055. doi:10.1016/j.addr.2008.02.012
Xia Y, Zhou Y, Tang Z (2011) Chiral inorganic nanoparticles: origin, optical properties and bioapplications. Nanoscale 3:1374–1382
Xu WW, Gao Y, Zeng XC (2015) Unraveling structures of protection ligands on gold nanoparticle Au68(SH)32. Sci Adv 1:e1400211. doi:10.1126/sciadv.1400211
Yong K-T, Roy I, Swihart MT, Prasad PN (2009) Multifunctional nanoparticles as biocompatible targeted probes for human cancer diagnosis and therapy. J Mater Chem 19:4655–4672. doi:10.1039/b817667c

Zeng C, Chen Y, Li G, Jin R (2014) Magic Size Au64(S-c-C6H11)32 nanocluster protected by cyclohexanethiolate. Chem Mater 26:2635–2641

Zeng C, Chen Y, Kirschbaum K, Appavoo K, Sfeir MY, Jin R (2015) Structural patterns at all scales in a nonmetallic chiral Au133(SR)52 nanoparticle. Sci Adv 1:e1500045

Zhang Z, Wang J, Chen C (2013) Near-infrared light-mediated nanoplatforms for cancer thermo-chemotherapy and optical imaging. Adv Mater 25:3869–3880. doi:10.1002/adma.201301890

Zhao P, Li N, Astruc D (2013) State of the art in gold nanoparticle synthesis. Coordin Chem Rev 257:638–665. doi:10.1016/j.ccr.2012.09.002

Zhou J, Ralston J, Sedev R, Beattie DA (2009) Functionalized gold nanoparticles: synthesis, structure and colloid stability. J Colloids Interface Sci 331:251–262. doi:10.1016/j.jcis.2008.12.002